Maximizing Line-of-Sight Coverage for mmWave Wireless LANs With Multiple Access Points

Yuchen Liu, *Graduate Student Member, IEEE*, Yubing Jian, Raghupathy Sivakumar, *Fellow, IEEE*, and Douglas M. Blough, *Senior Member, IEEE*

***Abstract*— In this paper, we investigate the optimal line-of-sight (LoS) coverage problem for multiple access point (multi-AP) mmWave wireless LANs in indoor scenarios. Due to the weak diffraction ability of mmWave signals at 60 GHz, maintaining LoS communications between APs and client devices is critical to achieve ultra-high data rates with mmWave communications. We focus on the use of multiple APs deployed to maximize LoS coverage in a target area, and we develop multi-AP placements that maximize LoS coverage by means of both analytical and algorithmic methods. We consider two main scenarios, which differ in their assumptions about knowledge of obstacles and clients. In a random-obstacle, random-client scenario, we derive the LoS-optimal positions of APs by solving a thinnest covering problem. For a fixed-obstacle, random-client scenario, we propose an efficient algorithm that produces a multi-AP placement, which is shown through simulation to provide near-optimal LoS coverage. Finally, through extensive ns-3 simulations based on the IEEE 802.11ad protocol and mmWave-specific channel models, we show that our multi-AP placements are significantly better than existing placement approaches, both in terms of LoS coverage and aggregate throughput.**

***Index Terms*— Millimeter wave, multiple APs, optimal placement, line-of-sight, blockage, performance study.**

I. Introduction

IN RECENT years, millimeter-wave (mmWave) communication has been studied extensively as a promising technology to deliver gigabit-per-second data rates for bandwidth-hungry applications such as virtual/augmented reality (VR/AR) and real-time streaming of ultra high-definition (UHD) television in indoor scenarios [1], [2]. The research community has focused on technical challenges that must be overcome to make indoor mmWave communication a reality. On the industry side, there are standardization efforts such as IEEE 802.11ad/ay [3] and Wireless Gigabit Alliance (WiGig), and some mmWave products operating on the 60 GHz frequency [4] are focused on enabling mmWave communication for indoor WLANs to support these emerging applications.

Manuscript received October 24, 2019; revised October 15, 2020, August 6, 2021, and October 15, 2021; accepted October 16, 2021; approved by IEEE/ACM TRANSACTIONS ON NETWORKING Editor K. Jamieson. This work was supported by the National Science Foundation under Award CNS-1813242 and Award CNS-2016381. *(Corresponding author: Yuchen Liu.)*

The authors are with the School of Electrical and Computer Engineering, Georgia Institute of Technology, Atlanta, GA 30332 USA (e-mail: yuchen.liu@gatech.edu).

Digital Object Identifier 10.1109/TNET.2021.3122378

To compensate for the poor propagation characteristics of mmWave signals as compared to lower-frequency signals, high-gain directional antennas are used on mmWave devices to reduce path loss. However, this makes mmWave communications susceptible to blockage effects [5], [6] from obstacles such as walls, cabinets and even human beings. As a result, line-of-sight (LoS) connectivity between access points (APs) and clients is critical to achieve good link performance, because mmWave signals experience very high penetration loss and reflection loss [7] in many non-LoS (NLoS) cases.

To illustrate the importance of LoS links, consider [8], where experiments were conducted to compare the throughput performance of 60 GHz transmissions for LoS and NLoS cases. The results of [8] show that in an open LoS area, 60 GHz WLAN can achieve more than 1.5 Gbps throughput even beyond typical AP-client separation distances; however, the throughput drops to very low values under NLoS conditions, which means that obstacles would effectively disconnect mmWave links. Another work evaluated a generic indoor path-loss model in the 60 GHz band for the LoS and NLoS cases in a laboratory scenario, where the path-loss exponents were measured as 2.0 and 5.4, respectively [9]. This means that for an AP-client separation between 5m and 12m, there is 23.76 dB to 36.69 dB loss of received signal strength in the NLoS case as compared to the LoS case. These measurements demonstrate that LoS links between APs and clients are required to achieve reliably high link data rates in typical indoor settings.

One common approach to improving performance for mmWave LANs is the use of multiple APs [10]–[19]. The general problem we consider herein is how to choose the positions of APs so as to achieve the best overall network performance. Due to the importance of LoS communication for mmWave frequencies, as highlighted above, we hypothesize that choosing AP positions in order to maximize LoS coverage will achieve the desired goal. Thus, the specific problem we consider, referred to as *the LoS-optimal placement problem*, is how to place APs in order to maximize LoS coverage within a target area. Some of the prior works on multiple AP placement do not factor in the LoS aspect and the ones that do only provide heuristic placement methods. Here, we propose placement algorithms specifically designed to maximize LoS coverage and we show through ns-3 simulations with mmWave-specific models that the constructed placements also maximize the network throughput.

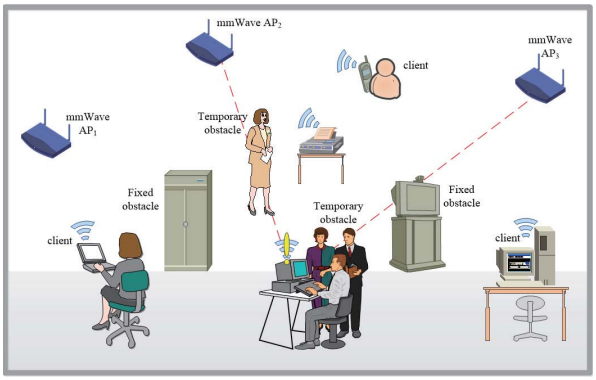

Fig. 1. Multi-AP mmWave wireless local-area network.

To be more specific, we consider two typical indoor scenarios: the random-obstacle, random-client (RORC) scenario and the fixed-obstacle, random-client (FORC) scenario.[1] In the RORC scenario without any obstacle or client information, we show that the LoS-optimal placement problem is equivalent to finding the AP placement that minimizes the maximum distance to any location in the room, which then maximizes the LoS coverage probability with random obstacles. By solving a thinnest covering problem, we solve this problem exactly to derive the LoS-optimal positions of multiple APs for arbitrary-sized rectangular rooms. In the FORC scenario where obstacles are fixed and their locations/dimensions are known, e.g. after furniture has already been placed in a room, we propose an efficient shadowing-elimination search (SES) algorithm that factors in the obstacles' information to optimize AP locations one by one. While the SES algorithm does not guarantee a LoS-optimal placement, we show through simulations that its performance is close to optimal for smaller problem sizes where the exact optimal solution can be determined through a brute force method.

The specific contributions of this work are as follows.

1) We introduce a mathematical framework to model obstacles in mmWave WLANs, and we derive the expected LoS probability and the shadowing-region area, which are key performance indexes to help determine the LoS-optimal AP placement.
2) We analytically derive the LoS-optimal AP placement by solving a thinnest covering problem in the scenario where obstacle and client locations are random and unknown.
3) We use geometric analysis to develop a shadowing elimination search (SES) algorithm, which optimizes LoS coverage within a sequential AP placement methodology, in the scenario where obstacles' sizes and locations are known.
4) While Contributions 1–3 assume rectangular rooms, we also design and evaluate methods to determine good AP placements in non-rectangular (but still rectilinear) rooms.
5) Through detailed ns-3 and Matlab simulations, we evaluate network performance and demonstrate that:
   - the proposed multi-AP placements produce significantly higher aggregate throughput compared to other placement approaches, which validates that LoS is a critical factor in achieving good performance in actual deployments, and
   - the proposed SES algorithm produces near-LoS-optimal AP placements for the simulated scenarios and has an enormous advantage in computational efficiency compared to brute-force search.

[1]Two other scenarios: random-obstacle, fixed-client (ROFC) and fixed-obstacle, fixed-client (FOFC) are special cases of RORC and FORC, respectively, and are also discussed in this work.

II. Related Work

To overcome blockages and improve coverage for mmWave WLANs, several approaches have been proposed in the literature and are discussed below.

Reflections. Previous work, e.g. [20]–[22], has considered the use of reflections to steer around obstacles, thereby avoiding blockages. For example, [20] showed that the use of reflected signals from the ceiling and walls can improve link quality in a 60 GHz WLAN system, while [21] proposed a solution where 60 GHz signals bounce off data center ceilings to avoid obstacles, and [22] studied the use of flat metal reflectors to improve network coverage in mmWave scenarios. However, reflections only maintain high signal-to-noise ratio off some materials, such as glass and certain metals, while for most surfaces, the reflection loss is severe at 60 GHz [23], which means that, in most cases, link quality over reflected signal paths is too low to support applications such as VR/AR and UHD video. The use of dedicated reflectors made of highly-reflective materials is another interesting research direction, which is complementary to the positioning of APs. For example, one can place a given number of APs so as to maximize LoS coverage and then deploy lower-cost dedicated reflectors to deal with remaining coverage gaps.

Reconfigurable Intelligent Surfaces. Reconfigurable intelligent surfaces (RISs) are an emerging technology that can be used as intelligent reflectors. RISs are low power devices that are composed of an array of electromagnetic elements, which, among other uses, allows them to reflect incoming signals outward at an angle different from the incident angle [24]. Thus, RISs can potentially expand coverage more than passive reflectors, for which the outgoing angle is fixed based on the direction of the incoming signal [25]. In relation to AP placement, however, RISs are complementary and can be used in a similar way to passive reflectors to augment coverage beyond what the APs can provide on their own.

Relay Nodes. Some other works, e.g. [26]–[29], use relay nodes to create multi-hop paths, where each individual link is LoS. If dedicated relay nodes are used, as in [26], this provides similar functionality to RISs, albeit at a higher power and with a mature technology. This approach is still complementary to AP placement, as discussed above. The 802.11ad specification [3] includes the capability to opportunistically use a node in the network as a single relay when a LoS path is blocked and several papers have considered how to best select opportunistic relay nodes [27], [28]. Unfortunately, opportunistic relays are not a general solution to the LoS coverage problem, because they are not always available when needed. In a novel design, [29] introduced a wireless system targeted at virtual reality applications by deploying a self-configurable mmWave mirror as a relay to redirect the signal

toward the receiver on the headset. However, that work only considers blockages caused by the user's own body and does not address blockage effects caused by furniture or other humans.

Infrastructure Mobility. In recent years, several works have considered the use of infrastructure mobility to improve network performance [30]–[33]. For mmWave WLANs specifically, [31] proposed a ceiling-mounted mobile AP model and explored the performance of different configurations of an AP mobility platform. Based on the model of [31], [32] presented a LoS prediction algorithm that dynamically identifies the target position on the mobility platform to maximize LoS connectivity. While AP mobility is an intriguing prospect, its relatively high cost compared to static APs together with the energy cost and delay of AP movement are challenges that still need to be addressed prior to its practical use.

Multiple APs. Because of ease of deployment and strong potential to improve LoS coverage, the use of multiple fixed APs to address the blockage and coverage problems has received a great deal of attention. Much of this work, e.g. [34], [35], has focused on protocol design and/or scheduling aspects but has not considered the multi-AP placement problem.

To our knowledge, the only works that have addressed the problem considered herein, i.e. multi-AP placement in indoor mmWave settings are [10]–[19]. Of these, [10]–[13] proposed specific placement schemes. In [10], the impact of base station deployment on LoS probability in 5G indoor scenarios was studied, but the only placement considered was deploying the base stations in a linear arrangement along the center line of a room. Other AP placement schemes were studied in [11]–[13]: [11] evaluated random placements, [12] considered randomly placing APs around the edges of a room, and [13] proposed evenly spacing APs around a room's edges. Each of the placement schemes considered in [10]–[13] is a heuristic scheme, whereas our approach is optimized for LoS coverage. A careful comparison of our approaches and these prior heuristics is provided in Sec. VII.

A number of the other papers on multi-AP placement did not consider the full impact of blockages [14]–[18], which is a critical issue in high-performance mmWave LANs. In [14]–[16], blockages were not considered at all and in [17], [18], blockages due to the user's own body were modeled stochastically but neither other human blockages nor obstacles such as furniture items were considered.

In [19], a custom hardware platform was used to measure the dominant reflectors in a target area, this information was fed into a ray tracer to predict link quality, and those predictions were then used to optimize AP placement. Due to its use of a specialized hardware platform, we are unable to include this approach in our comparative evaluations in Sec. VII. However, [19] differs from our approach in several key aspects. Importantly, due to the extremely high computational complexity of ray tracing, the AP placement of [19] is optimized only for a few common client locations rather than trying to maximize performance across the entire target area as we do herein. Also, whereas [19] requires detailed environment information collected by the custom hardware platform, our RORC placement approach only needs to know the room dimensions and does not require any information about the obstacle environment and our FORC placement approach only needs to know obstacle sizes and locations in addition to the room dimensions. In addition, the approach in [19] is more sensitive to environment dynamics, since the AP deployment highly depends on the sensed environment. Changes to the environment would then require redeployment of APs, which could be difficult and/or costly. By contrast, our RORC placement approach provides good performance over a wide range of obstacle environments, meaning that AP redeployment is not necessary after environment changes. Lastly, as noted in [19], its approach produces a good AP deployment when the environment is sparse and dominated by large reflectors, while this is not a requirement for our proposed approaches.

TABLE I
LIST OF NOTATIONS AND PARAMETERS

Notation	Meaning
$d_{i,j}$	Horizontal distance between node i and node j
w	Obstacle width, $w \sim \mathcal{N}(\mu_w, {\sigma_w}^2)$
l	Obstacle length, $l \sim \mathcal{N}(\mu_l, {\sigma_l}^2)$
c	Coordinates of obstacle center
h_o, θ	Obstacle height and orientation: $h_o \sim U(a_o, b_o), \theta \sim U(0, 2\pi)$
S_b	Blockage area caused by the obstacle
K	Number of obstacles
λ	Obstacle density in PPP
r_w, r_l, H_A	Room's width and length, and AP's height
h_c	Client height, $h_c \sim U(a_c, b_c)$
N	Number of APs
U, AP	The set of clients and APs
$P_{LoS_{i,j}}$	LoS probability between client i and AP j
u_i	The position of client i
Pos_j	The position of AP j
Rm	The ceiling plane of the room
D_n	Maximum horizontal distance with n APs
SA, SG	Shadowing area and shadowed grid

III. PRELIMINARIES

A. Blockage Model and Performance Metric Derivation

In this section, we use a stochastic geometric method to analyze blockage effects in indoor environments and evaluate the LoS performance theoretically. For convenience, Table I summarizes the notations used in the following sections.

To analytically model random obstacles from the 2-dimensional perspective, obstacles such as stationary furniture or temporarily stopped humans are assumed to form a Boolean scheme of rectangles [36]. We adopt this random object process from [36], in which the centers of the rectangles fall within the room and form a homogeneous Poisson point process (PPP) C of density λ, where λ is the mean number of obstacles in a unit square meter. The widths and lengths are assumed to be i.i.d. distributed and follow the normal distributions $W \sim \mathcal{N}(\mu_w, {\sigma_w}^2)$ and $L \sim \mathcal{N}(\mu_l, {\sigma_l}^2)$, respectively. The orientation distribution Θ of every obstacle is uniform over $[0, 2\pi]$. In this way, each obstacle B is completely characterized by the quadruple (c, w, l, θ), which is generated by sampling the distributions C, W, L, Θ.

Based on a Boolean scheme for obstacles in a 2D blockage model [37], we geometrically derive the blockage area S_b between client i and AP j in Eq. (1), where the LoS link is blocked when the center of obstacle $B_o(w, l, \theta)$ falls in S_b.

$$S_b(w, l, \theta, d) = d_{i,j} \cdot (|\cos\theta| \cdot w + |\sin\theta| \cdot l) + w \cdot l. \quad (1)$$

Then, considering the randomness of an obstacle's size, we can derive the expectation of the total number of obstacles K blocking the link between client i and AP j as:

$$E[K] = \int_{W_o}\int_{L_o}\int_{\Theta_o} \frac{1}{2\pi} S_b(w,l,\theta,d) f_{W_o}(w) f_{L_o}(l)\, dw\, dl\, d\theta = \frac{2d_{i,j}\cdot(\mu_w+\mu_l)}{\pi} + \mu_w\cdot\mu_l. \quad (2)$$

Now, we introduce the height effects of obstacles and extend the blockage model to 3 dimensions. It is known that an obstacle intersecting the link between client and AP with a horizontal length of d blocks the LoS path if and only if its height $h_o > h_x$, where $h_x = H_A + \frac{x}{d}\cdot(h_c - H_A)$, and H_A and h_c are the heights of AP and client ($H_A > h_c$), respectively.

Since the heights of obstacles are usually different in practice, we assume that the obstacle's height h_o follows the uniform distribution $H \sim U(a_o, b_o)$ in the remainder of this paper. Thus, in this 3-dimensional model, each obstacle B_o is characterized by the quintuple $\{c, w, l, h_o, \theta\}$. Let BL denote the event that the LoS path between the AP and the client is blocked. Assuming the height of client h_c also follows a uniform distribution $U(a_c, b_c)$, the conditional probability that an obstacle blocks the LoS path is:

$$\begin{aligned}\varepsilon &= \int_{-\infty}^{+\infty} P(\mathrm{BL}|h_c)\cdot f_H(h_c)\, dh_c \\ &= \int_{a_c}^{b_c} [1 - \int_0^1 \int_0^{y\cdot h_c + (1-y)H_A} f_H(h_o)\, dh\, dy] \cdot f_H(h_c)\, dh_c \\ &= 1 - \frac{2H_A - b_o - a_o}{2\cdot(b_c - a_c)} \cdot \ln(\frac{H_A - a_c}{H_A - b_c}). \end{aligned} \quad (3)$$

According to the PPP thinning property, the expected number of obstacles blocking a link in the 3D blockage model, $E[K]'$, is simply ε times the expectation in the 2D model, $E[K]$. Thus, the 3D LoS probability between client i and AP j is:

$$\begin{aligned} P_{LoS_{i,j}} = \exp\{-\lambda[&\frac{2d_{i,j}(\mu_w+\mu_l)}{\pi} \\ &- \frac{d_{i,j}(\mu_w+\mu_l)(2H_A - b_o - a_o)}{\pi(b_c - a_c)} \\ &\cdot \ln(\frac{H_A - a_c}{H_A - b_c}) - \frac{\mu_w\mu_l(2H_A - b_o - a_o)}{2\cdot(b_c - a_c)}) \\ &\cdot \ln(\frac{H_A - a_c}{H_A - b_c}) + \mu_w\mu_l]\}. \end{aligned} \quad (4)$$

According to Eq. (4), we observe that P_{LoS} increases monotonically with increasing H_A, which proves that the largest AP height provides the maximum LoS probability. Therefore, APs should be mounted on the ceiling of the room to achieve the best LoS performance. In what follows, we adopt this ceiling-mounted multi-AP architecture and focus on 2D deployment of APs in different indoor scenarios, since the 3D coordinates of APs can be easily obtained by adding the APs' height (i.e., the room's height).

B. Client and Mobility Model

In this work, we primarily consider unrestricted mobility patterns for clients, such that the clients can be located anywhere in the room. Under this assumption, our proposed RORC placement method (see Sec. IV) and FORC placement method (see Sec. V) can efficiently determine optimal AP locations that maximize network coverage. An alternative assumption, used for example in [19], is that clients move only between certain hotspot areas in the room. Our FOFC placement method (see Sec. V.E) can be considered to target this type of scenario. Although we do not discuss it herein, our FORC placement approach can also be applied to this scenario but with a smaller calculation space covering only the hotspot areas instead of the entire room, which would reduce its computation time accordingly. All evaluations in Sec. VII are conducted under the unrestricted mobility pattern assumption.

C. Practical Deployment Issues

As mentioned in Sec. II, our RORC placement approach only requires the dimensions of the room, while our FORC approach also requires obstacle sizes and locations. These approaches target different deployment scenarios. The RORC approach optimizes LoS coverage for random obstacle locations. Thus, its solution can be used when it is necessary to place APs in a room before obstacles, e.g. furniture items, are set up. In such a situation, obstacle locations are unknown and approaches that require such information are not viable. The RORC placement can also be used in a scenario where obstacle locations are expected to be changed frequently and AP redeployment is difficult and/or costly to perform. In this situation, it is preferable to have a fixed AP placement that can adapt to as many different obstacle configurations as possible, as opposed to a solution optimized for one initial obstacle configuration that could become highly sub-optimal after a configuration change. On the other hand, because our FORC placement approach requires obstacle locations, it targets scenarios where the APs are deployed *after* obstacles are already situated and either their locations are unlikely to change or they change very infrequently and maximizing performance is critical so that the cost of AP redeployment is considered secondary.

IV. Multi-AP Placement With Random Obstacles

In this section, we consider the RORC scenario, where obstacles and clients are randomly distributed, and the problem of maximizing LoS probability is equivalent to deploying APs so as to maximize the coverage of the target area.

A. Horizontal Distance Minimization

We assume that clients are randomly located and will find the closest APs for connection. Thus our objective is to deploy N APs in order to maximize the minimum LoS probability between each AP and its served users, and the problem can be formulated as:

$$\max_{Pos}\min_{i\in U}\{\max_{j\in AP} P_{LoS_{i,j}}\}, \quad \forall Pos \in Rm. \quad (5)$$

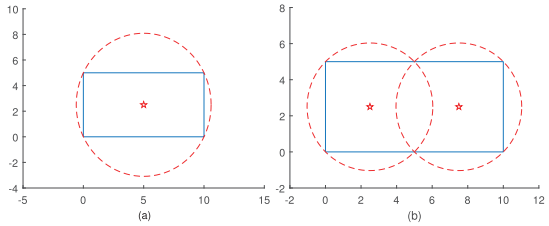

Fig. 2. Optimal positions of (a) 1 AP and (b) 2 APs. (e.g., $r_l = 10$m, $r_w = 5$m).

where Pos are the possible positions of the APs and should not be outside the target area. It can be seen from Eq. (4), that $P_{LoS_{i,j}}$ is inversely proportional to the distance, $d_{i,j}$, between the client and the AP. Therefore, we can reformulate the problem in Eq. (5) as finding the APs' positions that minimize the maximum horizontal distance between a random client and its served AP, which can be described as:

$$\arg\min_{Pos} \max_{i\in U}\{\min_{j\in AP} ||u_i - Pos_j||_2\}, \quad \forall u, Pos \in Rm. \quad (6)$$

Unfortunately, direct solution of Eq. (6) is impractical due to its non-convex nature. As a side note, however, with specific client hotspots in the room, the RORC scenario is transformed to a random-obstacle fixed-client (ROFC) scenario, and direct solution of Eq. (6) becomes feasible.

To solve the problem in Eq. (6) in the RORC scenario, we transform this multi-AP deployment (MD) problem into the *thinnest covering* (TC) problem [38], which is a classical mathematical problem that aims to find n congruent discs (circles) with the smallest radius r_n that cover a specific rectangle. Here, the goal of the thinnest covering problem is equivalent to our objective function in Eq. (6), which is trying to find optimal placement of n APs that minimizes the maximum horizontal distance (referred to as the achievable distance d_{ac}) between a random client and its serving AP. Here, r_n in TC problem is equal to d_{ac} in MD problem, and the center point of each circle in TC problem is the optimal position of each AP. In what follows, we derive the optimal placement for different numbers of APs.

B. Multi-AP Deployment Cases

In this part, we use both analytic methods and the simulated annealing approach in [38], [39] to solve the thinnest covering problem and derive the optimal locations of single or multiple APs in arbitrary-sized rectangular rooms.

First, we start with the simplest case when n is 1, i.e., deploying a single AP to achieve maximum LoS probability. Since ceiling-mounted APs are utilized, here we just focus on 2D placement of AP in RORC indoor settings. In a specific room with the length r_l and width r_w ($r_l \geq r_w$), the thinnest covering of a rectangle with one circle is shown in Fig. 2 (a), and the optimal position for single AP is $(\frac{r_l}{2}, \frac{r_w}{2})$. The achievable distance d_{ac}, i.e., the smallest radius of the circle r_1, is $\frac{1}{2}\sqrt{{r_l}^2 + {r_w}^2}$. This result shows that deploying the single AP in the center of the room provides the best LoS performance for randomly located clients.

In the 2-AP deployment case, the unique thinnest covering with two circles is shown in Fig. 2 (b), thus the optimal positions for two APs are $(\frac{r_l}{4}, \frac{r_w}{2})$ and $(\frac{3r_l}{4}, \frac{r_w}{2})$, and $d_{ac} = \frac{1}{4}\sqrt{{r_l}^2 + 4{r_w}^2}$.

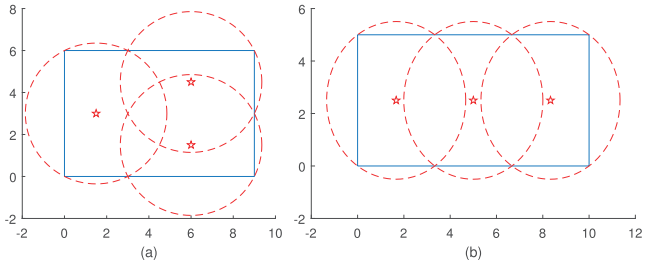

Fig. 3. Optimal positions of 3 APs (e.g. (a) $r_l = 9$m, $r_w = 6$m; (b) $r_l = 10$m, $r_w = 5$m).

Considering the 3-AP deployment, there are two types of thinnest covering in terms of room sizes (shown in Fig. 3). With different length-width ratios of the room, we derive the optimal positions for three APs as:

$$(x_i{}^*, y_i{}^*) = \begin{cases} (\frac{r_l}{6}, \frac{r_w}{2}), (\frac{2r_l}{3}, \frac{r_w}{4}), (\frac{2r_l}{3}, \frac{3r_w}{4}), & \text{if } \frac{r_l}{r_w} \leq \frac{3}{2}; \\ (\frac{r_l}{6}, \frac{r_w}{2}), (\frac{r_l}{2}, \frac{r_w}{2}), (\frac{5r_l}{6}, \frac{r_w}{2}), & \text{if } \frac{r_l}{r_w} > \frac{3}{2}. \end{cases} \quad (7)$$

The corresponding d_{ac} are $\frac{\sqrt{16{r_l}^4+40{r_l}^2{r_w}^2+9{r_w}^4}}{16r_l}$ and $\frac{\sqrt{{r_l}^2+9{r_w}^2}}{6}$, respectively.

In the same way, the optimal positions $(x_i{}^*, y_i{}^*)$ for 4-AP case are derived as follow:

$$\begin{cases} (\frac{r_l}{4}, \frac{r_w}{4}), (\frac{r_l}{4}, \frac{3r_w}{4}), (\frac{3r_l}{4}, \frac{r_w}{4}), (\frac{3r_l}{4}, \frac{3r_w}{4}), \\ \qquad\qquad \text{if } \frac{r_l}{r_w} \leq \sqrt{\frac{5+16\sqrt{10}}{15}}; \\ (K_{x1}, \frac{r_w}{2}), (\frac{r_l}{2}, 0), (\frac{r_l}{2}, r_w), (r_l - K_{x1}, \frac{r_w}{2}), \\ \qquad\qquad \text{if } \sqrt{\frac{5+16\sqrt{10}}{15}} < \frac{r_l}{r_w} < \frac{4}{\sqrt{3}}; \\ (\frac{r_l}{8}, \frac{r_w}{2}), (\frac{3r_l}{8}, \frac{r_w}{2}), (\frac{5r_l}{8}, \frac{r_w}{2}), (\frac{7r_l}{8}, \frac{r_w}{2}), \quad \text{if } \frac{r_l}{r_w} \geq \frac{4}{\sqrt{3}}, \end{cases} \quad (8)$$

where $K_{x1} = \sqrt{\frac{{r_w}^2}{36}(2\sqrt{\frac{{r_l}^2}{{r_w}^2}+3} - \frac{r_l}{r_w})^2 - \frac{{r_w}^2}{4}}$. The corresponding d_{ac} are $\frac{\sqrt{{r_l}^2+{r_w}^2}}{4}$, $\frac{2\sqrt{{r_l}^2+3{r_w}^2}-r_l}{6}$ and $\frac{\sqrt{{r_l}^2+16{r_w}^2}}{8}$, respectively. As Fig. 4 shows, there are 3 optimal deployment types for 4-AP case with respect to different length-width ratios of the room.

Considering the 5-AP and 6-AP deployment cases, the situation becomes more complicated since each of them has four thinnest coverings, which depend on the length-width ratio of the room (shown in Fig. 5 and Fig. 6). The interested reader is referred to Appendix A for the complete equations of optimal multi-AP positions for the 5-AP and 6-AP cases.

For optimal placement cases with more than 6 APs, we can use the same method to first solve the thinnest covering problem, and then derive the optimal positions of APs for different room length-width ratios. Actually, for all cases of RORC scenario reported on in later sections, deploying 6 APs provides more than sufficient performance gains and deploying additional APs provides little benefit in RORC scenarios.

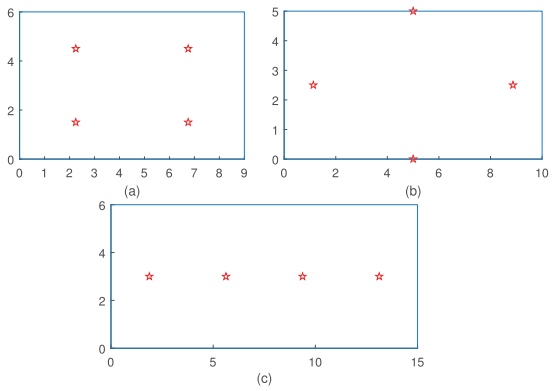

Fig. 4. Optimal positions of 4 APs (e.g. (a) $r_l = 9$m, $r_w = 6$m; (b) $r_l = 10$m, $r_w = 5$; (c) $r_l = 15$m, $r_w = 6$m).

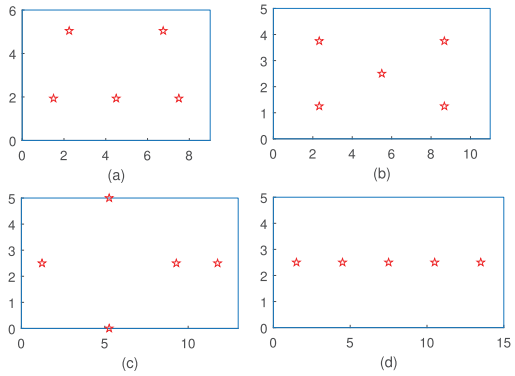

Fig. 5. Optimal positions of 5 APs (e.g. (a) $r_l = 9$m, $r_w = 6$m; (b) $r_l = 11$m, $r_w = 5$; (c) $r_l = 13$m, $r_w = 5$m; (d) $r_l = 15$m, $r_w = 5$m).

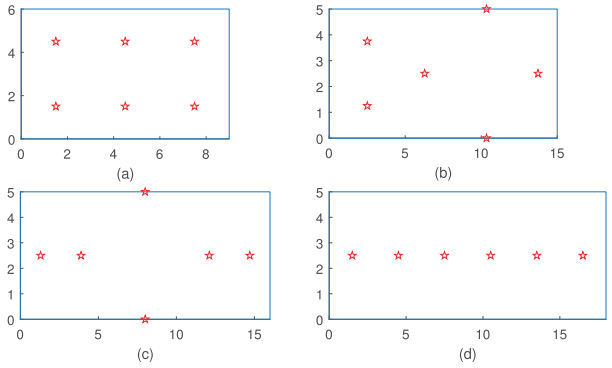

Fig. 6. Optimal positions of 6 APs (e.g. (a) $r_l = 9$m, $r_w = 6$m; (b) $r_l = 15$m, $r_w = 5$; (c) $r_l = 16$m, $r_w = 5$m; (d) $r_l = 18$m, $r_w = 5$m).

From the optimal placement results of 1∼6 APs, it is observed that there always exists one special deployment type that linearly arranges APs when one side of the room becomes sufficiently longer than the other side (see Fig. 3 (b), Fig. 4 (c), Fig. 5 (d), and Fig.6 (d)). The following theorem characterizes the conditions under which the linear arrangement becomes optimal for an arbitrary number of APs, N.

Theorem 1 (Linear arrangement condition): In a specific room ($r_l \times r_w \times r_h$) with N APs, if $r_l/r_w > N/\sqrt{3}$, the optimal deployment method is to linearly arrange APs on the ceiling and along the center line of the shorter edge of room, where the optimal position of i^{th} AP is $(\frac{(2i-1)r_l}{2N}, \frac{r_w}{2}, r_h)$.

Proof: According to the geometric analysis for thinnest covering of a longer rectangle, we can find the smallest

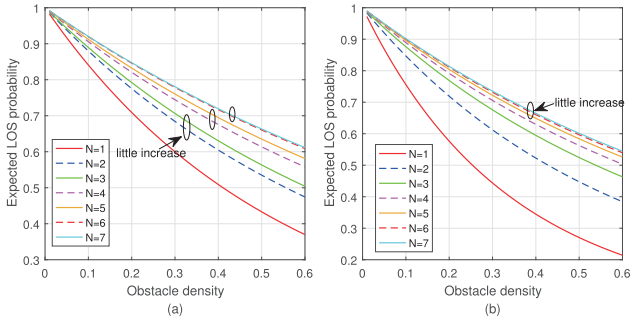

Fig. 7. ELP vs. obstacle density with varying number of APs (e.g., (a) $r_l = 9$m, $r_w = 6$m; (b) $r_l = 18$m, $r_w = 5$m).

radius of circles $r_n = d_{ac} \geq \frac{1}{2}\sqrt{(\frac{r_l}{N \cdot r_w})^2 + 1}$, and the linear covering like in Fig. 3 (b) is the only arrangement that attains the lower bound of r_n if $r_l/r_w > N/\sqrt{3}$. Then we can derive the y-axis coordinate of each AP must be in the middle of short edge of the room, and x-axis coordinate for i^{th} AP along the longer edge of room is $[(2i-1)r_l]/2N$. Since we adopt the ceiling-based APs to achieve better LoS performance (see Sec. III), the z-axis of each AP is obtained as r_h. □

C. Line-of-Sight Probability vs. Number of APs

Based on the preceding theoretical analysis of multi-AP deployment in RORC scenarios, here we investigate the performance benefits as the number of APs varies.

First, we derive the expected LoS probability (ELP) as a metric for subsequent evaluation. Since a randomly-located client can be viewed as a random point distributed in a circle with a radius of D_n (i.e., achievable distance d_{ac}), ELP of a random client and its connected AP is derived as:

$$\begin{aligned} ELP &= \int_0^{D_n} P_{LoS_{i,j}}(x) \cdot \frac{2x}{D_n^2} dx \\ &= \frac{2e^{-C_2}}{{C_1}^2 \cdot {D_n}^2} \cdot (1 - e^{-C_1 \cdot D_n} - C_1 \cdot D_n \cdot e^{-C_1 \cdot D_n}) \end{aligned} \tag{9}$$

where $C_1 = \frac{2\varepsilon \cdot \lambda \cdot (\mu_l + \mu_w)}{\pi}$, $C_2 = \varepsilon \cdot \lambda \cdot \mu_l \cdot \mu_w$, $P_{LoS_{i,j}}$ has been derived in Eq. (4), and D_n is the maximum horizontal distance which can be obtained from Sec. IV-B in terms of the number of APs n.

We evaluate the expected LoS probability with respect to the number of APs and the obstacle density. Fig. 7 (a) shows the results in a 9m × 6m room, and we find that deploying an odd number of APs brings smaller performance improvement than deploying an even number of APs, e.g., deploying 3 APs brings little performance increase compared with deploying 2 APs, but there is a relatively larger improvement when moving from 3 APs to 4 APs. Note also that the performance gains become much smaller with a higher number of APs, and this result is more obvious in Fig. 7 (b) with a "longer" room (18m × 5m), especially when the number of APs is larger than 5, the sixth AP only brings a performance increase of less than 1%.

In addition, we also investigate how room sizes affect the LoS performance. With a specific obstacle density ($\lambda = 0.3$) and room's length-width ratio ($r_l/r_w = 2.5$), Fig. 8 shows that

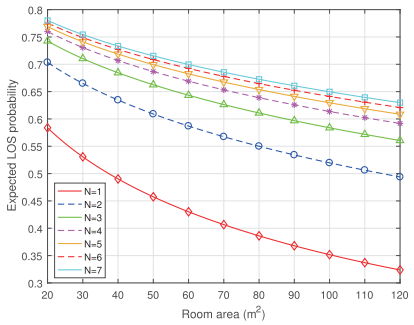

Fig. 8. ELP vs. room size with varying number of APs.

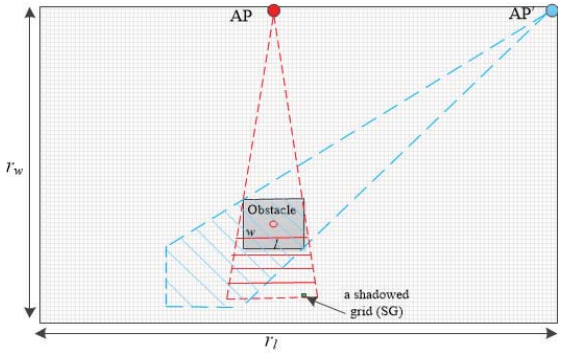

Fig. 9. Top view of the shadowing region (areas filled by red or blue lines) caused by a single obstacle.

the ELP decreases as the room size increases with different numbers of APs. This is because the maximal horizontal distance (D_n) increases with a larger room, which results in a higher probability of experiencing blockage between an AP and its clients. On the other hand, as the number of APs increases with a specific room area, the performance improvement brought by a higher number of APs is marginal, where the average performance increases over different room areas from 2^{nd} AP to 7^{th} AP are 40.21%, 10.56%, 4.43%, 2.17%, 1.43% and 1.06%, respectively. Considering the cost of commercial mmWave AP devices, such as TP-Link Talon AD7200 Multi-Band Wi-Fi Router at $350 [4], the second "$350" brings 40.21% potential performance increase, but the sixth or seventh "$350" only brings around 1% improvement, which is in accordance with *the law of diminishing marginal utility*.

Note that the discussion of diminishing returns on the number of APs applies only to the case where obstacle locations are *unknown* (the RORC scenario). The conclusion listed here, i.e. that there is almost no benefit beyond 5 APs for the room sizes studied, do *not* necessarily hold when obstacle locations are *known* (the FORC scenario). Evaluation of that scenario is the topic of the next section.

V. Multi-AP Placement With Fixed Obstacles

In this section, we consider the fixed obstacle scenario, where furniture items, such as tables, cabinets or other objects with a minimum height,[2] have been placed in a room and their locations and sizes are known. Under this assumption of fixed and known obstacles in indoor settings, we investigate how to deploy APs to provide better LoS communications. Most of this section, considers the FORC case, where client locations are unknown (random) but Sec. V.E considers the FOFC case, where client locations are also fixed and known.

A. Shadowing Area Minimization

In the FORC scenario, achieving the best LoS coverage with multiple APs requires deploying APs so as to minimize the shadowing regions (SRs) caused by the obstacles. This problem can be formulated as:

$$\arg\min_{Pos} A\Big(\bigcup_{i\in Obs} SR_i\Big), \forall Pos \in Rm \tag{10}$$

[2]Here the object with the height larger than general height of client is considered as the obvious obstacle, since objects with very small heights will have no effect on LoS paths between ceiling-mounted APs and clients.

where SR_i is the SR caused by obstacle i, $A(\cdot)$ represents the area of a region, and each Pos is one possible combination of positions of the APs. Here, the union of SRs is taken to eliminate overlapping SRs of different obstacles.

Fig. 9 shows an example of a SR caused by a fixed obstacle. The shape and size of the SR is determined by several factors, such as the size of obstacle and the relative positions of the AP and the obstacle. Here, we make the assumption that obstacles in the room have only two orientations: 0° and 90°, which means that the edges of obstacle will be parallel with the walls. This assumption is reasonable in practice since we typically deploy furniture in the same direction as one of the walls in the room.

To solve Eq. (10) and find the placement of APs, we introduce a *grid-based shadowing search* (GSS) method to calculate the shadowing area, where the main idea is to first divide the rectangle (see Fig. 9) into a large number of small grid elements with side length l_g.[3] A grid element is referred to as a *shadowed grid*, or SG, if its center point is in the shadowing region. The SR is then simply the set of SGs. For a single obstacle and AP, a grid element is shadowed if its center point falls inside a shadowing polygon formed by the AP and obstacle. The detailed geometric analysis of this point existence problem can be found in Appendix B.

B. Single AP Case

For a single AP with a given position, the overall SR can be obtained by finding the SR for each individual obstacle and then taking the union of the SRs. Since the number of possible positions for one AP is the number of grid elements, it is practical to solve Eq. (10) by computing the SR for each possible AP position and selecting the position that has the SR with the smallest area. Algorithm 1 shows the pseudocode to compute the overall SR for one AP position. The method GSSFunction() computes the SR for one obstacle by doing the SG calculation described above for each grid element and placing each SG into the SR (denoted by SG_i in the pseudocode). Repeating this for every obstacle (Line 2) and eliminating duplicates (Lines 5-6) produces the overall SR (SG_{new} in the pseudocode), which is finally used to compute the shadowing area for the given AP position (Line 10). Although not shown in the pseudocode, Algorithm 1 is called

[3]A smaller l_g provides more accurate results but has higher computational cost.

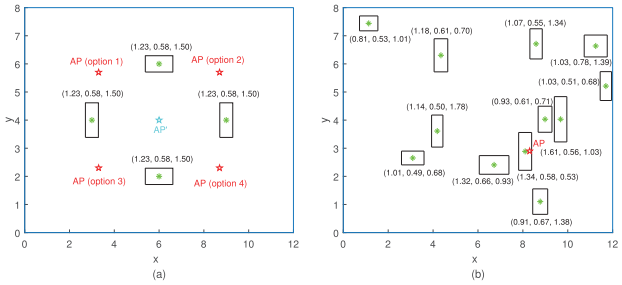

Fig. 10. Optimal position of a single AP for (a) a symmetrically deployed case and (b) a randomly deployed case (the data around each obstacle represents its length, width and height).

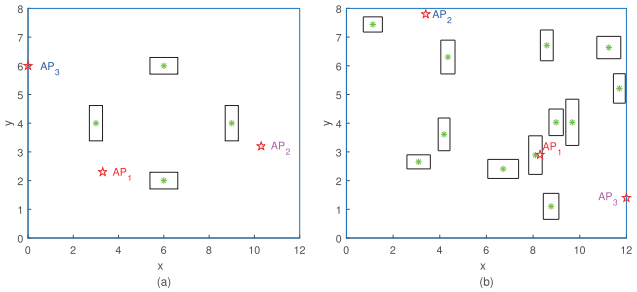

Fig. 11. Positions of 3 APs from SES algorithm for the (a) symmetrically deployed case and randomly deployed case of Fig 10.

for each possible AP position and the best AP position is determined from Eq. (10).

Algorithm 1 Finding the Union of SRs With Multiple Obstacles

Input: Obs (obstacles' positions), pos (AP's position), G (grid set), l_g (grid length), prm (includes r_w, r_l, H_A, size of each obstacle)
Output: SA_u

```
SG_new=[]; // init the shadowed-grid set
for each obstacle i ∈ Obs do
  [SA_i, SG_i] = GSSFunction(Obs(i), pos, G, prm);
  for each grid j ∈ SG_i do
    if (j ∉ SG_new) then
      SG_new.add(G(j));
    end if
  end for
end for
SA_u=size(SG_new) · l_g^2;
return SA_u, SG_new;
```

Fig. 10 shows several examples and their optimal AP placements. Fig. 10(a) shows an example where the four obstacles have the same sizes and are symmetrically located. If the obstacles' height is 1.5m, as shown in the figure, there are four equivalent positions (shown by red stars) to optimally deploy the AP, but if the obstacles' height is 2.0m, there is only one optimal position of the AP (shown by the blue star). This example shows that the heights of obstacles can have a significant impact on optimal AP deployment. Fig. 10(b) shows another example, where multiple obstacles with different sizes are randomly distributed. For this example, there is only one optimal position of the AP (shown by the red star). From these examples, we observe that the AP deployment in FORC scenarios is clearly different from RORC scenarios, where the optimal solution for this room size places the AP in the center of the room.

C. Multi-AP Case

In this part, we consider the multi-AP placement in FORC scenarios. The optimal positions of multiple APs could be found using the same method as the single-AP case, but the number of position combinations for multiple APs makes this approach impractical when the number of APs is more than two. Therefore, we propose a shadowing-elimination search (SES) heuristic for the multi-AP case.

Algorithm 2 summarizes the steps of the SES algorithm. First, considering all grid elements in the room, Algorithm 1 is executed to get the union of the SRs for each possible *single AP* position (Lines 3-5). Thus, the first time through the for loop, the first AP is placed in the optimal position for the single AP case (Lines 6-7). Before starting to find the second AP's position, the grid set G is updated to the SG set of the first AP, which means that SRs that have been eliminated by previously selected APs are not considered in the next iteration of the loop (Line 8). This means that the second AP will be placed at the position that eliminates the largest area of the SRs that remain after the first AP is placed. Then, the third AP is placed to minimize the remaining SRs given the first two APs' positions. If, after any iteration of the loop, all SRs are eliminated, the process stops (Line 9). Otherwise, the process continues until all N APs are placed in this manner.

Algorithm 2 SES: Shadowing-Elimination Search

Input: Obs, l_g, prm, N
Output: P_{ap}

```
1: G=[all grids ∈ Rm]; // first consider all grid elements
2: for each AP i from 1 to N do
3:   for each pos of AP i do
4:     [SA_{u_i}, SG_i]=FindUnionSR(Obs, pos, G, l_g, prm);
5:   end for
6:   AP_i=arg min{SA_{u_i}};
7:   P_ap.add(AP_i);
8:   G=[grids in SG_i]; // update G
9:   if G = ∅ break;
10: end for
11: return P_ap;
```

Fig 11 shows the placement of multiple APs resulting from the SES algorithm for the same examples as in Fig 10. By deploying 3 APs in each case, the remaining shadowing areas are 0.11m^2 and 0.56m^2, respectively, which eliminates substantially more shadowing area as compared to the single AP results in Fig. 10, where the remaining shadowing areas were 16.01m^2 and 20.07m^2, respectively.

D. Blockage-Free, Multi-AP mmWave WLANs

As the number of APs increases, eventually the SES algorithm will entirely eliminate the remaining shadowing area to achieve full coverage, i.e., the mmWave network scenario becomes blockage-free and randomly-located clients can always have LoS connections.

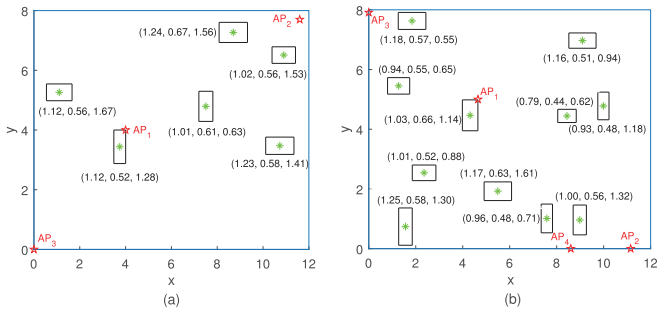

Fig. 12. Deployment of multiple APs to achieve blockage-free conditions (the data around each obstacle represents its length, width and height). (a) 3-APs deployment case; (b) 4-APs deployment case.

A straightforward extension of the SES algorithm can place as many APs as necessary to make the environment blockage-free. This extended algorithm simply places APs one by one according to the SES algorithm, checks the remaining shadowing region after each new AP is placed, and halts when the remaining shadowing region is empty. Fig. 12 shows two examples of placing multiple APs to achieve the blockage-free condition. It is observed that 3 and 4 APs are required in Fig. 12 (a) and (b), respectively.

E. Multi-AP Placement in FOFC Scenarios

If client locations or hotspots are also fixed and known, the FORC scenario becomes a fixed-obstacle-fixed-client (FOFC) scenario. The SES algorithm could still be used for this case, however minimizing the shadowing regions from the entire room's perspective does not necessarily produce a good solution for a given set of client locations. In the worst case, even if the remaining shadowing regions are small, all clients might be located within them and none of the clients will achieve LoS. When client locations are known, we can directly evaluate whether a particular AP placement provides full LoS coverage for those known client locations.

Algorithm 3 shows our approach to generating an AP placement in FOFC scenarios. This is referred to as Algorithm "check LoS status", or CLS for short. This algorithm will both find a better AP placement and run more efficiently than the SES algorithm, because it relies on a simpler line-of-sight calculation instead of the more complicated shadowing region calculation of SES. The first time through the outer for loop, we set the first AP's position to the one that provides LoS connections for the maximum number of client locations (Lines 3-10). Then, to take care of the remaining NLoS clients, we find the next AP's position that can provide LoS connections for the maximum number of remaining NLoS clients with respect to the first generated AP (Lines 4, 14), and so on. Note that if there are multiple positions of APs that can provide LoS connections for the maximum number of client locations (Line 10), we choose the one that has the minimum achievable distances for its LoS client locations (Line 12), because shorter distances produce better link performances.

The CLS algorithm can also be extended to find a multi-AP placement that achieves a blockage-free condition in FOFC scenarios. Similar to how Algorithm 2 was extended to achieve blockage-free conditions, the CLS extension repeatedly places APs according to Algorithm 3 until all client locations have a

Algorithm 3 CLS: Check Line-of-Sight Status

Input: Obs, $clients$, prm, N
Output: P_{ap};
1: $Nset$.add(all $clients$); // init an NLoS set
2: **for** each AP i from 1 to N **do**
3: **for** each pos of AP $i \in Rm$ **do**
4: **for** each client location $j \in Nset$ **do**
5: **if** CheckLoS(i, j, Obs, prm)=$true$ **then**
6: $LoSNum_p = LoSNum_p + 1$;
7: **end if**
8: **end for**
9: **end for**
10: $AP_i = \arg\max_p\{LoSNum\}$;
11: **if** AP_i.size > 1 **then**
12: $AP_i = \arg\min_i\{\max_j d_{i,j}\}$;
13: **end if**
14: $Nset$.rmv(all LoS client locations of AP_i);
15: P_{ap}.add(AP_i);
16: **if** $Nset = \emptyset$ **break**;
17: **end for**
18: **return** P_{ap};

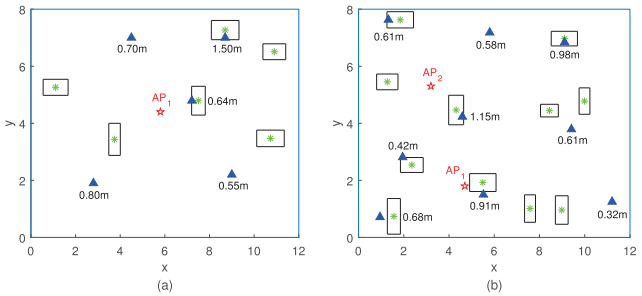

Fig. 13. Examples of multi-AP placement in the FOFC scenario (the blue triangles and numbers denote the clients' locations and heights). (a) 1-AP deployment case; (b) 2-APs deployment case.

LoS path to at least one AP. Example results of this extension of Algorithm 3 are shown in Fig. 13 with the same obstacles as in Fig. 12 and fixed client locations (shown with blue triangles and their heights). In these examples, 1 AP and 2 APs are required in Fig. 13 (a), (b), respectively, to achieve LoS coverage for all client locations. Compared to the multi-AP placements in FORC scenarios where 3 APs and 4 APs are deployed (see Fig. 12), these examples show that we can achieve blockage-free operation with fewer APs if the clients' locations are known and fixed.

VI. AP Placement in Non-Rectangular Rooms

In general, the proposed analytical model and algorithms in this paper can also generate AP placements for non-rectangular rooms if the rooms are combinations of several rectangular rooms. For example, "L-shaped" ("U-shaped") rooms[4] can be divided into two (three) rectangular room sections. One simple approach would be to generate the optimal (near-optimal) positions of APs for each rectangular section separately and combine the solutions. In the remainder of this section, we modify our previously proposed algorithms to

[4]In practice, L-shaped and U-shaped rooms are two most typical non-rectangular rooms, thus we focus on these types.

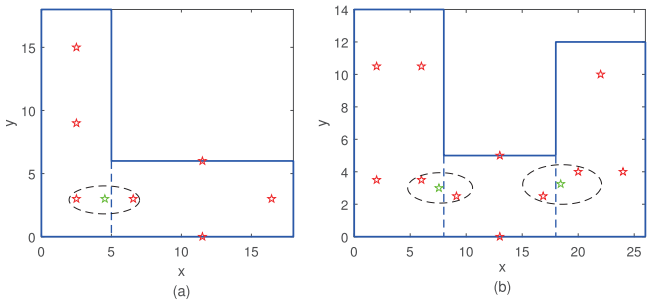

Fig. 14. Examples of multi-AP placements in (a) L-shaped room and (b) U-shaped room (the green star denotes the new AP that replaces original two close APs).

determine whether we can produce better placements for these non-rectangular rooms, as compared to the simple approach.

A. AP Placement in RORC Scenarios

In RORC scenarios, we first optimally deploy APs for each rectangular room section by using the method of Sec. IV-B. Then, where two rectangular sections come together, if two APs are very close to each other, i.e., they have large overlapping coverage areas, we try to improve the placement by replacing the two APs with a single AP placed at the relative center position of the two APs. However, before accepting the new placement, we should evaluate the performance loss by doing this adjustment, since there is a trade-off between the expected LoS performance and the number of placed APs.

According to Eq. (9), we know that ELP is closely related to the achievable distance D_{ac}, and if the original AP placement is adjusted in a rectangular room, we should first recompute new D'_{ac} in Eq. (11) to evaluate the expected LoS performance.

$$D'_{ac} = \max_{i \in U}\{\min_{j \in AP'} ||u_i - Pos_j||_2\}, \ \forall u, Pos \in Rm_k, \quad (11)$$

where AP$'$ is the new AP set in rectangular room k. Then, we further calculate the updated ELP in non-rectangular room based on Eq. (9) and the total probability theorem as:

$$ELP' = \frac{1}{\sum_i S_i} \cdot \sum_i [\frac{S_i \cdot 2e^{-C_2}}{{C_1}^2 \cdot {D'_{ac_i}}^2} \cdot (1 - e^{-C_1 \cdot D'_{ac_i}} - C_1 \cdot D'_{ac_i} \cdot e^{-C_1 \cdot D'_{ac_i}})], \quad (12)$$

where C_1, C_2 are the same parameters as in Eq. (9), and S_i is the product of length and width of rectangular room section i. In this way, we can get the estimated performance of the modified placement, which uses fewer APs but might cause a performance loss as compared with the original placement. Fig. 14 shows two examples of multi-AP placements in L-shaped and U-shaped rooms. With the obstacle density of $\lambda = 0.2$, if we replace two APs with the new AP (shown with the green star) at the joint place of two rectangular rooms, the expected LoS probability loss for "L-shaped" and "U-shaped" are 2.73% and 0.83%, respectively, but we save 1 AP and 2 APs for the two cases.

In particular, before doing the adjustment with fewer APs, we should compare the LoS performance of the adjusted case with that of all possible separate-optimal arrangements, and then choose the case which has best performance as the optimal solution to deploy APs. With the same number of APs as the adjusted case (e.g., N APs), the number of possible separate-optimal deployments is:

$$\begin{cases} N-1, & \text{L}-\text{shaped} \\ \frac{1}{2} \cdot N^2 - \frac{3}{2} \cdot N + 1, & \text{U}-\text{shaped}. \end{cases} \quad (13)$$

For the example shown in Fig. 14(a), only 6 APs are required after doing the adjustment, and the ELP comparisons between the adjusted case (AD) and all separate-optimal deployment approaches are shown in Table II, where "$n-m$" denotes the case that there are n APs and m APs optimally deployed in the left and bottom rectangular rooms, respectively. The table shows that the "3-3" case shows the best performance for both obstacle densities (λ). Therefore, in this L-shaped room with 6 APs, we should optimally deploy 3 APs in each rectangular room section instead of doing the adjustment shown in Fig. 14(a).

In the U-shaped room example (Fig. 14(b)), we do similar performance comparisons among all 28 separate-optimal arrangement cases, and the result shows that "3-2-4" case has the highest ELP. Table III shows the performance comparisons between the "3-2-4" case and the adjusted case shown in Fig. 14(b), and we observe that "3-2-4" case is still superior to the adjusted case, even though the performance difference is less than 1% with lower obstacle densities. However, this difference becomes more obvious as the obstacle density increases.

By leveraging the coverage of an AP that is at the intersection of two rectangular room sections, sometimes the adjusted case can outperform all separate-optimal placements with the same number of APs. For example, Fig. 15 shows a case where we replace two APs close to the intersection point with one AP (shown with the green star), and slightly shift other APs in the bottom rectangular room. Table IV shows that the adjusted case is superior to all separate-optimal cases for this example.

To summarize, before doing an adjustment to save APs in a non-rectangular room, it is necessary to evaluate the per-

TABLE II
PERFORMANCE COMPARISON WITH DIFFERENT DEPLOYMENT CASES

Case	1-5	2-4	3-3	4-2	5-1	AD
$ELP_{\lambda=0.2}(\%)$	82.02	86.64	87.85	87.75	85.24	85.48
$ELP_{\lambda=0.4}(\%)$	68.07	75.25	77.28	77.13	73.03	73.26

TABLE III
PERFORMANCE COMPARISON WITH DIFFERENT DEPLOYMENT CASES

Obstacle density	$\lambda = 0.1$	$\lambda = 0.2$	$\lambda = 0.4$
ELP (%) ("3-2-4" case)	93.42	87.32	76.37
ELP (%) (Adjusted case)	93.09	86.71	75.32

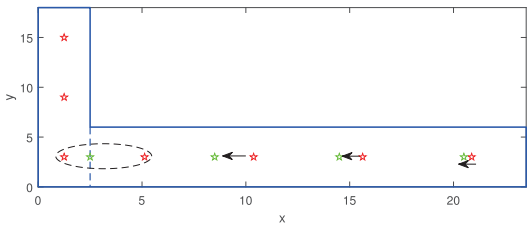

Fig. 15. An example of adjusted case in a L-shaped room (the green stars denote the adjusted locations of APs).

TABLE IV
PERFORMANCE COMPARISON WITH DIFFERENT DEPLOYMENT CASES

Case	1-5	2-4	3-3	4-2	5-1	AD
ELP$_{\lambda=0.2}$(%)	84.97	86.92	86.70	84.76	77.55	87.10
ELP$_{\lambda=0.4}$(%)	72.75	75.59	74.97	71.91	61.36	76.12

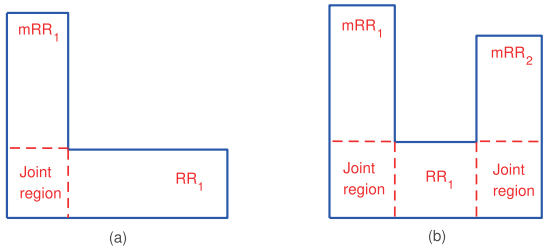

Fig. 16. The joint regions in (a) L-shaped room and (b) U-shaped room.

formance between the adjusted case and all separate-optimal placements with the same number of APs. The adjusted placement can be chosen if it outperforms all other evaluated placements. Otherwise, the separate-optimal placement with the best performance should be adopted.

B. AP Placement in FORC Scenarios

In FORC scenarios, after running the SES algorithm to generate an AP placement for each rectangular room section, we cannot replace two closer APs with one AP at the intersection points as in RORC scenarios, because even a small change of an original AP's position might generate a large shadowing region, especially for the case where each rectangular room section has achieved the blockage-free condition. Therefore, we provide a new version of the SES algorithm, referred to as mSES, to generate AP placements in non-rectangular rooms. mSES is shown in Algorithm 4.

To achieve blockage-free operation, we first divide the non-rectangular room into several rectangular room sections (RRs), and find the joint regions (JR) of these RRs (shown in Fig. 16) (Line 1), such that we can handle the independent and dependent regions, respectively. Note that these joint regions (JRs) are physically contained in one of the RRs according to the rectangle-separation step, and those RRs containing JRs are referred to as master RRs (mRR). Next, the algorithm in Sec. V-D is executed to generate the AP placement for each mRR (e.g. mRR$_1$ in Fig. 16(a) or mRR$_1$ and mRR$_2$ in Fig. 16(b)) (Lines 2-4). Since the APs that are in the joint regions have already eliminated some of the shadowing regions for adjacent non-mRR (e.g., RR$_1$ in Fig. 16 (a) and (b)), we only consider the remaining shadowed grids of the non-mRRs (Lines 5-11), which avoids considering the shadowing regions that have already been eliminated in previous steps. Finally, for the non-mRRs, the SES algorithm is executed with respect to their respective remaining shadowing regions, and similar to Algorithm 2, the AP placement result is obtained after eliminating all shadowing regions (Lines 12-21).

Algorithm 4 Multi-AP Deployment in Non-Rectangular Rooms

Input: Obs, l_g, prm
Output: P_{ap}; $NumAP$
1: RR = Separation(non-rec Rm); // rectangle-separation step
2: **for** each mRR$_i$ $\in RR$ **do**
3: $P_{ap}(i)$=Ext-Algorithm2($Obs, l_g, params$);
4: **end for**
5: **for** each non-mRR$_j$ $\in RR$ **do**
6: G_j=[all grids $\in$ non-mRR$_j$];
7: **for** each AP $\in P_{ap}$ & $\in JRs$ **do**
8: $[SA_{u_j}, SG_j]$=FindUnionSR(Obs, pos, G_j, l_g, prm);
9: G_j=[grids in SG_j]; // record remaining SRs
10: **end for**
11: **end for**
12: **for** each non-mRR$_j$ $\in RR$ **do**
13: $k = 1$;
14: **while** $k > 0$ **do**
15: **for** each position p of AP k **do**
16: $[SA_{u_k}, SG_k]$=FindUnionSR(Obs, p, G_j, l_g, prm);
17: **end for**
18: AP_k=arg min$\{SA_{u_k}\}$;
19: P_{ap}.add(AP_k);
20: G_j=[grids in SG_k]; // update G_j
21: **if** $SA_{u_k} = 0$ **then break**;
22: **end while**
23: **end for**
24: **return** P_{ap}, $NumAP$ = size(P_{ap});

VII. PERFORMANCE STUDY

In this section, we report the results of simulation-based analyses of our AP placement approaches. After introducing the ns-3 based simulation platform, we present an evaluation of the network performance of our approaches and several baseline methods under a variety of mmWave LAN scenarios.

A. mmWave Indoor Network Model

To perform realistic simulations of mmWave networks, we modified the 802.11ad model in the ns-3 simulator [40]–[42], which includes the 802.11ad packet error rate (PER) model and bit error rate (BER) vs. SNR lookup tables for 60 GHz mmWave PHY layers. We made substantial changes to the simulator, including adding a cuboid-based obstacle model, an accurate LoS-determination function, a sparse cluster-based channel model, and support for multiple APs.

Our evaluations were done with an obstacle model that includes both furniture-type obstacles and human obstacles with the following features: 1) obstacles are modeled as cuboids and placed on the floor; 2) the center of each obstacle follows a Poisson point process with a specific density λ; 3) the widths, lengths, and heights of furniture-type obstacles follow the truncated normal distributions W$\sim \mathcal{TN}$(0.56, 0.08, 0.25, 1.25), L$\sim \mathcal{TN}$(1.08, 0.18, 0.5, 1.75), and H$\sim \mathcal{TN}$(0.9, 0.6, 0.5, 2.0)),[5] respectively, while the widths, lengths, and heights of human obstacles follow the truncated normal distributions W$\sim \mathcal{TN}$(0.25, 0.05, 0.1, 0.5), L$\sim \mathcal{TN}$(0.5, 0.1, 0.2, 0.9), and H$\sim \mathcal{TN}$(1.65, 0.20, 1.4, 1.9)); 4) each obstacle's orientation follows a uniform distribution $\Theta \sim \mathcal{U}(0, \pi)$. Finally, wireless device locations are uniformly distributed across the (x, y) dimensions of the room and device heights follow the uniform distribution $\mathcal{U}$(0.3, 1.5). These parameters are derived based

[5]The unit for all distance values is meters.

on [31], [43] and the enterprise cubicle scenario defined in [44], which use real-life lab environments as guiding examples.

To accurately model mmWave indoor channels, we adopted the Saleh-Valenzuela (S-V) model for 60 GHz office/lab environments from [45], which characterizes the multipath components (MPCs) arriving in clusters, formed by multiple reflections from the objects in the vicinity of a transmitter or receiver. In the S-V model, clusters and rays within each cluster arrive according to Poisson processes with different rates and have inter-arrival times that are exponentially distributed. We employ the S-V channel model in our ns-3 simulator and all modeling parameters (e.g., cluster/ray decay time, arrival rate, K-factor, etc.) are chosen from [45]–[47], which are derived based on measurements in real 60 GHz office/lab network environments. Due to the use of narrow-beam directional antennas (see Fig. 1 in Appendix C), the expected number of clusters and rays at each receiver location are set as 2 and 6, respectively, which is in accordance with [47] where measurements from narrow-beam directional antennas were conducted. We consider three different reflective coefficient (R_0) distributions in the channel model, which are all normal distributions: $\mathcal{N}(0.35, 0.1)$ (Low-R case), $\mathcal{N}(0.6, 0.1)$ (Medium-R case), and $\mathcal{N}(0.85, 0.1)$ (High-R case). These are intended to model scenarios with objects having low, medium, and high reflectivities, respectively.

B. Performance in RORC Scenarios

In this subsection, we evaluate the network performance of our LoS-optimal multi-AP placement approach in RORC scenarios, and with the simulation parameters detailed in Sec. VII-A. Here, LoS probability and aggregate throughput are considered as the main metrics for evaluation. First, considering a rectangular room of size 12m $\times$ 8m, we compare the network performance of the LoS-optimal multi-AP placement (see Sec. IV-B) against that of four placement methods from the literature, namely 1) random placement [11], 2) linear arrangement [10], where APs are placed along the line perpendicular to and bisecting the shorter edge of the room, 3) edge placement [12], where APs are randomly placed on the edges of the room, and 4) perimeter placement [13], where APs are evenly spaced along the edges of the room.

With obstacle density $\lambda = 0.3$, Fig. 17 illustrates the LoS probability and throughput performance for 1 to 6 APs and for the three different reflective coefficient distribution cases considered. Fig. 17(a) shows that the LoS probability of the LoS-optimal placement approach outperforms the other four placement methods. For example, with 3 APs, the LoS probability is 5%, 19%, 14%, and 5% higher than linear, edge, perimeter and random placements, respectively.

Fig. 17 also shows that the throughput performance for the Low-R and Medium-R cases is quite consistent with LoS probability[6] (compare Fig. 17(a) with Fig. 17(b)-(c)) and, therefore, the percentage increases in throughput are nearly identical to the increases in LoS probability. For the High-R Case (see Fig. 17(d)), all placement approaches have higher throughput than they did in the Low-R and Medium-R Cases,

[6]The application data rate was set to 4 Gbps in ns-3, so the throughput range in our heat maps has this as the maximum throughput value.

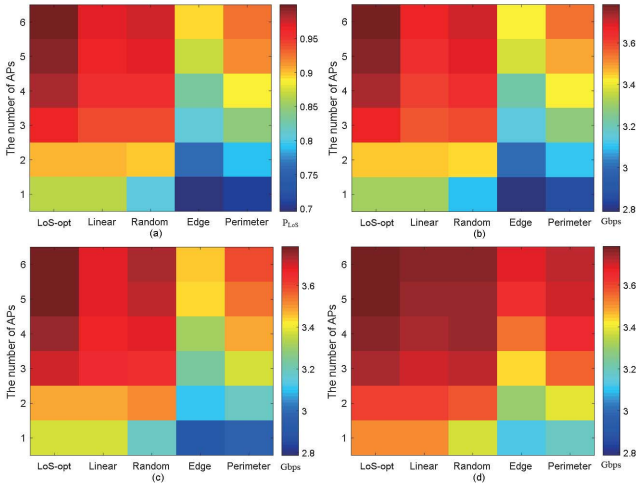

Fig. 17. Comparison of placement methods for different numbers of APs with $\lambda = 0.3$: (a) LoS probability; (b) throughput for Low-R case; (c) throughput for Medium-R case; (d) throughput for High-R case.

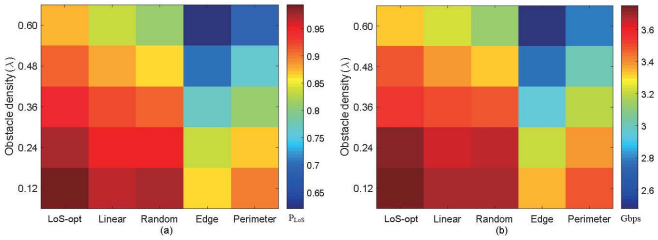

Fig. 18. Comparison of placement methods for different obstacle densities with 3 APs and medium reflectivity: (a) LoS probability and (b) throughput.

but throughput is still highly correlated with LoS probability. Throughput is higher overall, because with highly-reflective objects in the room, stronger multi-path components exist and NLoS paths can also contribute to the network performance. However, even in this case, our LoS-optimal placement approach still outperforms the other placement methods by 4–12%, which validates that maximizing LoS probability is an effective strategy to improve performance in mmWave WLANs.

Next, we vary the obstacle density and evaluate the network performance for the different AP placement approaches. For 3 APs and the Medium-R case, Fig. 18 shows that the LoS-optimal placement outperforms the other placement approaches in both LoS coverage and throughput performance. Compared to the next best approach at each obstacle density studied, the LoS-optimal placement is about 5% better at low obstacle densities and more than 20% better at high obstacle densities, in terms of both LoS probability and throughput.

We also investigate more deeply the LoS-optimal placement by varying obstacle density and the number of APs for the Medium-R case. The results are shown in Fig. 19. The figure shows that both LoS probability and throughput performance decrease when the obstacle density becomes higher due to more severe blockage effects. A higher number of APs can partially alleviate these effects but the increase in both LoS probability and throughput is less than 1% when going from 5 to 6 APs at the highest obstacle density. This is consistent with our theoretical analysis in Sec. IV-C.

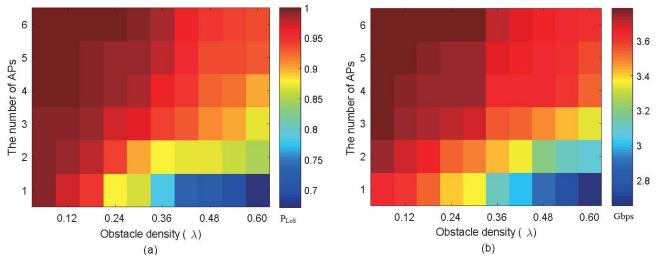

Fig. 19. Performance of our LoS-optimal placement with medium reflectivity: (a) LoS probability vs. obstacle density and number of APs and (b) throughput vs. obstacle density and number of APs.

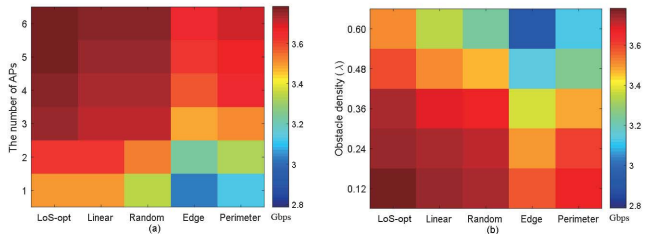

Fig. 20. Throughput comparison of placement methods for modified channel model with medium reflectivity: (a) varying number of APs ($\lambda = 0.3$) and (b) varying obstacle density (3 APs).

Finally, we evaluate the impact of modifying the expected number of clusters N_{cl} in the S-V channel model. Recall that we set N_{cl} to 2 based on [47], which matched our assumption of a highly directional antenna on the APs. Here, we modify N_{cl} to 4 in accordance with [45], which was based on an omnidirectional AP antenna. Fig. 20 shows the throughput performance vs. number of APs and obstacle density for the LoS-optimal approach and comparison placements with this modified channel model. It is observed that throughputs are higher overall, as compared to the results in Fig. 17 and Fig. 18 under the default channel model, because a larger N_{cl} produces stronger multi-path components such that NLoS paths can also contribute to the network performance. However, even with this modified channel setting, we observe that the LoS-optimal placement method still outperforms the other approaches, particularly with fewer APs and higher obstacle density.

C. Performance in FORC Scenarios

In this subsection, we evaluate the network performance of the SES algorithm for multi-AP placement in FORC scenarios, and with the simulation parameters detailed in Sec. VII-A. Here, our primary metrics are the all-client LoS rate (ALR), Gbps-throughput percentage (GTP), and the number of APs needed to achieve blockage-free conditions, i.e. where there is a LoS connection from every point in the room to at least one AP. For each data point, 500 simulation runs are conducted where, for each simulation run, clients (wireless devices) are uniformly distributed across the room. ALR is defined as the percentage of simulation runs where every client has a LoS connection to at least one AP. GTP is defined as the percentage of clients across all simulation runs that achieve at least 1 Gbps throughput, which is a typical goal for a mmWave link. The SES algorithm is compared against the same approaches from the literature considered in the previous subsection (which do not take into account obstacle locations) and also against

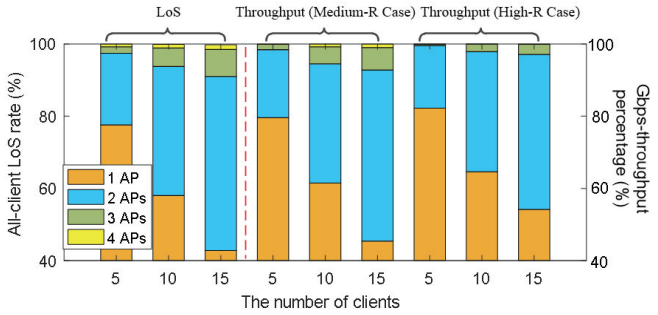

Fig. 21. Network performance of our SES algorithm vs. the number of APs and clients with $\lambda = 0.2$.

a brute-force placement approach that considers all possible multi-AP placements for a given set of obstacles but can take multiple days to run for moderately complex scenarios.

Fig. 21 shows the network performance provided by the SES algorithm with different numbers of APs and clients. The figure shows that an ALR of over 90% is achieved when deploying 3 APs even with 15 randomly located clients, which is a huge improvement compared to the single AP case. The figure also shows that 4 APs are sufficient to effectively achieve blockage-free conditions, i.e. an ALR over 99.99% with up to 15 clients. When considering throughput, the figure shows that the measured throughput of the Medium-R case closely tracks the LoS performance,[7] and when 3–4 APs are placed by the SES algorithm, almost all clients achieve at least 1 Gbps throughput in the network. For the High-R case, note that Gbps performance can be achieved by a high percentage of clients with only two APs even with 15 clients. This is a result of both maximizing LoS coverage with the SES algorithm and the potentially beneficial NLoS paths caused by highly reflective objects in the High-R case.

Next, we compare the SES algorithm with other AP placement approaches. Fig. 22 reports the results for the Medium-R case and 10 randomly located clients. It is observed that our SES algorithm outperforms other approaches by around 7–22%, 15–20%, 13–18% and 10–17% with 1–3 APs, respectively. This is because the SES algorithm exploits environment information to produce customized multi-AP placements. Additionally, we observe that the second and third APs substantially improve network performance since the SES algorithm intelligently finds the next AP location to minimize performance loss based on the current blockage effects, while other approaches fail to reach the performance of the SES algorithm with 3 APs even when deploying 4 APs. We see that fewer AP are required to achieve very high performance with the SES deployment approach for both the default S-V channel model (Channel 1) and the modified S-V channel model with $N_{cl} = 4$ (Channel 2).

To further evaluate the SES algorithm, we compare its network performance to that of a brute-force placement algorithm that considers all possible placements of multiple APs and chooses the one with the smallest shadowing region (this is equivalent to solving Eq. (10) in a brute-force manner). The brute-force algorithm can sometimes achieve blockage-free conditions with fewer APs than the SES algorithm,

[7]Here, we omit the throughput result for the Low-R case, because it is nearly identical to the LoS performance.

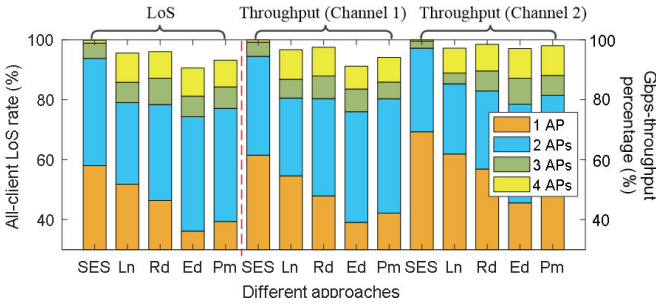

Fig. 22. Network performance of the SES algorithm and other placement methods with $\lambda = 0.2$, 10 clients, and the Medium-R case ("Ln", "Rd", "Ed" and "Pm" denote linear, random, edge and perimeter placement approaches).

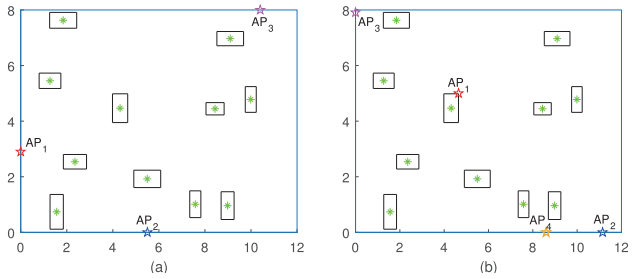

Fig. 23. Multi-AP placements to achieve blockage-free conditions: ((a) brute-force algorithm and (b) SES algorithm.

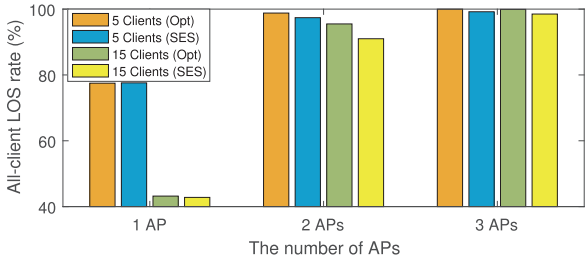

Fig. 24. ALR comparison between brute-force and SES algorithms.

because it considers all possible placement combinations of APs while the SES algorithm optimizes the placement sequentially. Fig. 23 shows an example scenario where, to produce a blockage-free condition, the brute-force algorithm needs only 3 APs, whereas the SES algorithm requires 4 APs. However, as will be presented later, the brute-force algorithm sometimes takes multiple days to determine a placement while the SES algorithm time complexity is linear in the number of APs (for a fixed number of obstacles) and linear in the number of obstacles (for a fixed number of APs).

To provide a more comprehensive comparison, Fig. 24 shows the ALR of the two algorithms for the scenario case shown in Fig. 23. The figure shows that the performance of the SES algorithm is very close to that of the brute-force algorithm with the same number of APs. Even though one more AP is sometimes required by the SES algorithm to entirely eliminate the shadowing region after deploying the third AP (as shown in Fig. 23 (b)), its ALR is above 98.5% without the 4^{th} AP, and the remaining shadowing area is only 0.73 m^2 on average, which is very close to full coverage.

We also compared the number of APs needed to achieve blockage-free conditions with the SES and brute-force

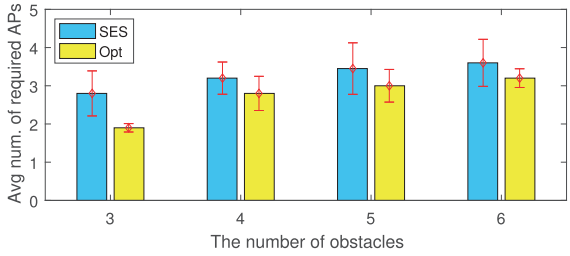

Fig. 25. Average number of APs to achieve blockage-free conditions vs. number of obstacles.

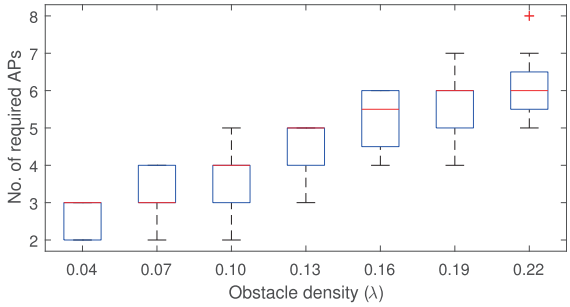

Fig. 26. Number of APs to achieve blockage-free conditions with the SES algorithm vs. obstacle density.

TABLE V
COMPUTATION TIME FOR SES ALGORITHM AND OPTIMAL (BRUTE-FORCE) METHOD IN HOURS

No. of Obstacles	2	4	6	8	10
Optimal Alg.	0.23	2.57	13.21	36.32	82.35
SES Alg.	0.18	0.26	0.48	0.59	0.68

algorithms. Since it is too time consuming to get the brute-force results with a large number of obstacles (see below), here we considered cases with a small number of obstacles only. Fig. 25 shows that the number of APs needed with the SES algorithm is close to that of the brute force algorithm, and as the obstacle scale increases, the gap between SES and brute force algorithms becomes smaller. In addition, Fig. 26 shows a box-plot of the number of APs needed to achieve full coverage with the SES algorithm, which shows that the increase in the required number of APs becomes smaller as the obstacle density increases.

Lastly, we evaluated the running times of the SES and brute force algorithms vs. the number of obstacles.[8] As shown in Table V, the running time of the brute force algorithm increases dramatically when there are more than 4 obstacles in FORC scenarios, but the computation time of the SES algorithm increases roughly linearly with the number of obstacles, which shows its huge advantage in computation efficiency.

D. The Impact of Human Blockages

In this part, we investigate the impact of human blockages in the network scenarios with proposed multi-AP placements, where mmWave signals could be blocked by fixed obstacles (e.g., furniture) and/or human bodies. For a fixed mean obstacle density of $0.2/m^2$ and a varying density of human

[8]Running times were evaluated on an Intel(R) Core(TM) i5-6200U 2.3GHz CPU workstation with 2 cores and 4 logical processors.

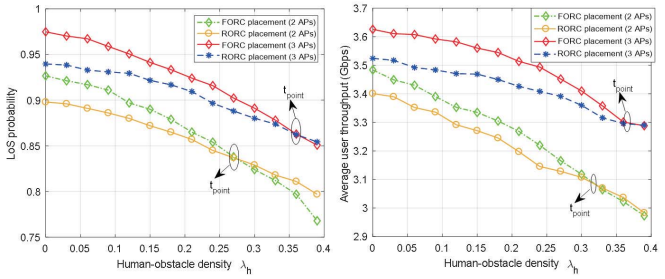

Fig. 27. Network performance vs. human-obstacle density with $\lambda = 0.2$ and medium reflectivity.

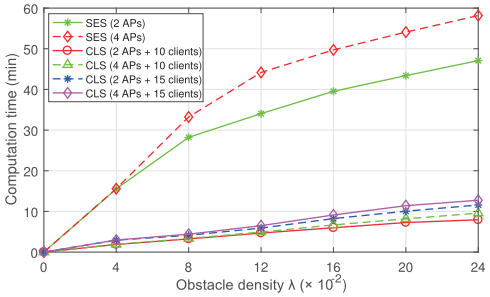

Fig. 28. Computation time for SES algorithm and CLS algorithm.

obstacles, we evaluated the effectiveness of our placement approaches in terms of both LoS probability and throughput (see Fig. 27). Here, the average user throughput indicates the average of the data bytes received per second by all client samples at different locations. Specifically, we evaluate the performance of two proposed placement approaches: RORC placement, i.e. the LoS-optimal placement from Sec. IV and FORC placement, i.e. the SES algorithm.

From Fig. 27, we observe that the human blockages have less impact on the RORC placement than on the FORC placement. As the density of human obstacles, λ_h, increases, the network performance drops a little due to the increased human-blockage effects, but the FORC placement scheme still works fairly well when λ_h is not very high. However, at a threshold point (t_{point}) as the human-obstacle density becomes much higher than the fixed-obstacle density, the RORC placement provided better performance, because the scenario tends to be more like RORC, i.e. the randomly located human obstacles dominate. In the simulations we performed, t_{point} always occurs at fairly high human-obstacle densities, which means that RORC placement does a better job only when there are a large number of human obstacles, e.g., around 25–30 humans for the 2-AP case and even more with 3 APs. Thus, for lab-type environments where a smaller number of people is expected, the FORC placement is still preferable to the RORC placement when obstacle locations are known.

E. Performance of CLS Algorithm in FOFC Scenarios

Here, we evaluate the CLS algorithm (see Algorithm 3), tailored to determine a good AP placement in FOFC scenarios, and compare it to the SES Algorithm that does not make use of client locations. Fig. 28 shows the computation times of the SES and CLS algorithms[8]. Note that the running time of the SES algorithm is about 5 times as long as that of the CLS algorithm. The CLS algorithm not only runs faster than the SES algorithm but, due to its use of client locations, it produces a better placement than the SES algorithm, which tries to produce a good placement for randomly located clients. Averaged over all data points shown in Figure 28, the CLS algorithm resulted in 99.69% of the clients achieving LoS with at least one AP, while the SES algorithm only achieved LoS for 92.36% of the clients.

VIII. Conclusion

This paper addressed the optimal line-of-sight (LoS) coverage problem for multiple access point (multi-AP) mmWave wireless LANs in indoor scenarios. We considered two typical indoor scenarios, one where nothing is known about potential obstacles and a second where obstacle locations and sizes are known. For the former case, we analytically derived the AP placement that maximizes the LoS probability for a randomly located client as a function of the number of APs and the dimensions of the target area. For the latter case, we proposed the shadowing-elimination search algorithm that minimizes the remaining LoS-uncovered area as APs are placed one by one in the target area. Through IEEE 802.11ad simulations at 60 GHz with ns-3, both the LoS coverage and the network throughput of the proposed AP placement approaches were shown to be superior to those of previously proposed placement methods across a variety of indoor scenarios.

There are several opportunities for future work based on our results. It would be interesting to explore a combination of APs *and* strategically placed reflectors or RISs to increase network performance while lowering cost and improving adaptability to dynamic environments. Additionally, since this work focused exclusively on rectilinear rooms and cuboid-shaped obstacles, LoS-optimal placements under more general assumptions, e.g. rooms with curved walls and/or irregularly shaped obstacles, remain an open problem.

Appendix A
Optimal Locations for 5–6 APs in RORC Scenarios

As shown in Fig. 6, the optimal positions $(x_i{}^*, y_i{}^*)$ of 5 APs are derived as:

$$\begin{cases} I\text{: } (\frac{r_l}{6}, K_{y1}), (\frac{r_l}{2}, K_{y1}), (\frac{5r_l}{6}, K_{y1}), (\frac{r_l}{4}, K_{y2}), (\frac{3r_l}{4}, K_{y2}), \\ \qquad\qquad \text{if } \frac{r_l}{r_w} \le 2.02; \\ II\text{: } (K_{x2}, \frac{r_w}{4}), (K_{x2}, \frac{3r_w}{4}), (\frac{r_l}{2}, \frac{r_w}{2}), (r_l - K_{x2}, \frac{r_w}{4}), \\ \qquad (r_l - K_{x2}, \frac{3r_w}{4}), \qquad \text{if } 2.02 < \frac{r_l}{r_w} \le 2.35; \\ III\text{: } (K_{x3}, \frac{r_w}{2}), (K_{x4}, 0), (K_{x4}, r_w), (K_{x5}, \frac{r_w}{2}), \\ \qquad (r_l - K_{x3}, \frac{r_w}{2}), \qquad \text{if } 2.35 < \frac{r_l}{r_w} \le \frac{5}{\sqrt{3}}; \\ IV\text{: } (\frac{r_l}{10}, \frac{r_w}{2}), (\frac{3r_l}{10}, \frac{r_w}{2}), (\frac{r_l}{2}, \frac{r_w}{2}), (\frac{7r_l}{10}, \frac{r_w}{2}), (\frac{9r_l}{10}, \frac{r_w}{2}), \\ \qquad\qquad \text{if } \frac{r_l}{r_w} > \frac{5}{\sqrt{3}}. \end{cases} \quad (14)$$

where

$$\begin{cases} K_{y1} = \sqrt{{D_{(1)}}^2 - \frac{{r_l}^2}{36}},\ K_{y2} = r_w - \sqrt{{D_{(1)}}^2 - \frac{{r_l}^2}{16}}, \\ K_{x2} = \sqrt{{D_{(2)}}^2 - \frac{{r_w}^2}{16}}, K_{x4} = 2\sqrt{{D_{(3)}}^2 - \frac{{r_w}^2}{4}} + D_{(3)}, \\ K_{x3} = \sqrt{{D_{(3)}}^2 - \frac{{r_w}^2}{4}},\ K_{x5} = 3\sqrt{{D_{(3)}}^2 - \frac{{r_w}^2}{4}} + 2D_{(3)}, \end{cases} \tag{15}$$

where $D_{(i)}$ $(1 \le i \le 4)$ is the achievable distance d_{ac} of *Type* i, and $D_{(1)}$ is the smallest positive real root of the equation in Theorem 5 of [31], $D_{(2)} = \frac{1}{6}\sqrt{5{r_l}^2 - 2r_l\sqrt{4{r_l}^2 - 9{r_w}^2}}$, $D_{(3)} = \frac{1}{16}(3\sqrt{{r_l}^2 + 8{r_w}^2} - r_l)$, and $D_{(4)} = \frac{1}{10}\sqrt{{r_l}^2 + 25{r_w}^2}$.

In the 6-AP deployment case, we have four different types which are shown in Fig. 7, and the optimal positions of these 6 APs are derived as follows:

$$\begin{cases} I\text{:} & (\frac{r_l}{6}, \frac{r_w}{4}), (\frac{r_l}{6}, \frac{3r_w}{4}), (\frac{r_l}{2}, \frac{r_w}{4}), (\frac{r_l}{2}, \frac{3r_w}{4}), (\frac{5r_l}{6}, \frac{r_w}{4}), \\ & (\frac{5r_l}{6}, \frac{3r_w}{4}), \quad \text{if } \frac{r_l}{r_w} \le 2.92; \\ II\text{:} & (K_{x6}, \frac{r_w}{4}), (K_{x6}, \frac{3r_w}{4}), (K_{x7}, \frac{r_w}{2}), (K_{x8}, 0), \\ & (K_{x8}, r_w), (K_{x9}, \frac{r_w}{2}), \quad \text{if } 2.92 < \frac{r_l}{r_w} \le 2 + \frac{\sqrt{5}}{2}; \\ III\text{:} & (K_{x10}, \frac{r_w}{2}), (K_{x11}, \frac{r_w}{2}), (\frac{r_l}{2}, 0), (\frac{r_l}{2}, r_w), (r_l - \\ & K_{x11}, \frac{r_w}{2}), (r_l - K_{x10}, \frac{r_w}{2}), \text{ if } 2 + \frac{\sqrt{5}}{2} < \frac{r_l}{r_w} \le \frac{6}{\sqrt{3}}; \\ IV\text{:} & (\frac{r_l}{12}, \frac{r_w}{2}), (\frac{r_l}{4}, \frac{r_w}{2}), (\frac{5r_l}{12}, \frac{r_w}{2}), (\frac{7r_l}{12}, \frac{r_w}{2}), (\frac{3r_l}{4}, \frac{r_w}{2}), \\ & (\frac{11r_l}{12}, \frac{r_w}{2}), \quad \text{if } \frac{r_l}{r_w} > \frac{6}{\sqrt{3}}. \end{cases} \tag{16}$$

where

$$\begin{cases} K_{x6} = \sqrt{{D_{(2)}}^2 - \frac{{r_w}^2}{16}}, K_{x7} = 2\sqrt{{D_{(2)}}^2 - \frac{{r_w}^2}{16}} + \\ \qquad \sqrt{{D_{(2)}}^2 - \frac{{r_w}^2}{4}}, \\ K_{x8} = {D_{(2)}}^2 + 2\sqrt{{D_{(2)}}^2 - \frac{{r_w}^2}{16}} + 2\sqrt{{D_{(2)}}^2 - \frac{{r_w}^2}{4}}, \\ K_{x9} = r_l - \sqrt{{D_{(2)}}^2 - \frac{{r_w}^2}{4}},\ K_{x10} = \sqrt{{D_{(3)}}^2 - \frac{{r_w}^2}{4}}, \\ K_{x11} = 3\sqrt{{D_{(3)}}^2 - \frac{{r_w}^2}{4}}. \end{cases} \tag{17}$$

Here the achievable distance of *Type* I $D_{(1)} = \frac{1}{12}\sqrt{4{r_l}^2 + 9{r_w}^2}$, $D_{(2)}$ of *Type II* is the smallest positive root of following equation:

$$2\sqrt{4{D_{(2)}}^2 - {r_w}^2} + 2D_{(2)} + \sqrt{4{D_{(2)}}^2 - 1/4{r_w}^2} - r_l = 0, \tag{18}$$

and $D_{(3)} = \frac{1}{30} \cdot (4\sqrt{{r_l}^2 + 15{r_w}^2} - r_l)$, $D_{(4)} = \frac{1}{12}\sqrt{{r_l}^2 + 36{r_w}^2}$.

APPENDIX B
GRID-BASED SHADOWING SEARCH METHOD

In this section, we present the grid-based shadowing search (GSS) method mentioned in this paper. According to AP's position and obstacle's information, we can determine whether each grid is shadowed or not by judging if its center point exists in the shadowing polygon. The shape and size of shadowing polygon are determined by the obstacle's size and relative position between AP and obstacle. According to the geometric analysis, we divide all possible relative positions between the AP and obstacle into 9 types, and Algorithm 1 shows how to use above basic information to obtain the shadowing area.

In the "input" arguments, Obs and AP are the 2-D coordinates of obstacle and AP, respectively; w, l, h, θ are the width, length, height and orientation (only consider 0° and 90°) of the known obstacle; r_w, r_l, H_A are the width, length and height of the room; l_g is the side length of each grid, and it can be set as 0.05∼1 to get a relative accurate result in a 12×8 room; G is a grid set which includes all grids in the room by default. In the "output" arguments, we obtain the shadowing area SA and shadowed-grid set SG, which contains all grid elements in the shadowing region.

Algorithm 5 Grid-Based Shadowing Search Method

Input: $Obs(x_o, y_o)$, $AP(x_p, y_p)$, w, l, h, θ, r_w, r_l, H_A, l_g, G
Output: SA, SG

if $\theta = 90°$ **then**
  SwitchValue(l, w); // assume $l(w)$ along $x(y)$ axis
end if
Define points $O_1(x_o + \frac{l}{2}, y_o + \frac{w}{2})$, $O_2(x_o + \frac{l}{2}, y_o - \frac{w}{2})$, $O_3(x_o - \frac{l}{2}, y_o + \frac{w}{2})$, $O_4(x_o - \frac{l}{2}, y_o - \frac{w}{2})$;
$\delta = H_A/(H_A - h)$;
for each grid $G_i(x_g, y_g) \in G$ **do**
  // **Type 1**:
  if $x_p < x_o - \frac{l}{2}$, & $y_p > y_o + \frac{w}{2}$ **then**
    $l_1(AP, O_4)$, $l_2(AP, O_1)$, $l_3(O_1, O_4)$; // 3 line functions
    $d = \delta \cdot length(AP, O_2)$;
    $K = (O_2.y - y_p)/(O_2.x - x_p)$;
    $x_e = \frac{d}{\sqrt{K^2+1}} + x_p$, $y_e = \frac{K \cdot d}{\sqrt{K^2+1}} + y_p$;
    if $G_i \in Area(O_1, O_2, O_3, O_4)$ **then continue**; // on the obstacle
    if $x_g \le x_e$ & $y_g \in [max\{l_1(x_g).y, y_e\}$, $min\{l_2(x_g).y,\ l_3(x_g).y\}]$ **then**
      SG.add(G_i);
    end if
  // **Type 2**:
  else if $x_p \in [x_o - \frac{l}{2}, x_o + \frac{l}{2}]$ & $y_p > y_o + \frac{w}{2}$ **then**
    $l_1(AP, O_3)$, $l_2(AP, O_1)$;
    $d = \delta \cdot (y_p - y_o + \frac{w}{2})$;
    $y_e = y_p - d$;
    if $G_i \in Area(O_1, O_2, O_3, O_4)$ **then continue**;
    if $y_g \in [y_e, min\{l_1(x_g).y,\ l_2(x_g).y,\ y_o + \frac{w}{2}\}]$ **then**
      SG.add(G_i);
    end if
  // **Type 3**:
  else if $x_p > x_o + \frac{l}{2}$ & $y_p > y_o + \frac{w}{2}$ **then**
    $l_1(AP, O_3)$, $l_2(AP, O_2)$, $l_3(O_3, O_2)$;
    $d = \delta \cdot length(AP, O_4)$;
    $K = (O_4.y - y_p)/(O_4.x - x_p)$;
    $x_e = -\frac{d}{\sqrt{K^2+1}} + x_p$, $y_e = -\frac{K \cdot d}{\sqrt{K^2+1}} + y_p$;
    if $G_i \in Area(O_1, O_2, O_3, O_4)$ **then continue**;
    if $x_g \ge x_e$ & $y_g \in [max\{l_2(x_g).y,\ y_e\}$,

$min\{l_1(x_g).y,\ l_3(x_g).y\}]$ **then**
SG.add(G_i);
end if
// **Type 4**:
else if $x_p > x_o + \frac{l}{2}$ & $y_p \in [y_o - \frac{w}{2}, y_o + \frac{w}{2}]$ **then**
$l_1(AP, O_1)$, $l_2(AP, O_2)$;
$d = \delta \cdot (x_p - x_o + \frac{l}{2})$;
$x_e = x_p - d$;
if $G_i \in Area(O_1, O_2, O_3, O_4)$ **then continue**;
if $x_g \in [x_e,\ x_o + \frac{l}{2}]$ & $y_g \in [l_2(x_g).y,\ l_1(x_g).y]$ **then**
SG.add(G_i);
end if
// **Type 5**:
else if $x_p > x_o + \frac{l}{2}$ & $y_p < y_o - \frac{w}{2}$ **then**
$l_1(AP, O_1)$, $l_2(AP, O_4)$, $l_3(O_1, O_4)$;
$d = \delta \cdot length(AP, O_3)$;
$K = (O_3.y - y_p)/(O_3.x - x_p)$;
$x_e = -\frac{d}{\sqrt{K^2+1}} + x_p$, $y_e = -\frac{K \cdot d}{\sqrt{K^2+1}} + y_p$;
if $G_i \in Area(O_1, O_2, O_3, O_4)$ **then continue**;
if $x_g \geq x_e$ & $y_g \in [max\{l_2(x_g).y,\ l_3(x_g).y\},$
$min\{l_1(x_g).y,\ ye\}]$ **then**
SG.add(G_i);
end if
// **Type 6**:
else if $x_p \in [x_o - \frac{l}{2}, x_o + \frac{l}{2}]$ & $y_p < y_o - \frac{w}{2}$ **then**
$l_1(AP, O_4)$, $l_2(AP, O_2)$;
$d = \delta \cdot (y_o + \frac{w}{2} - y_p)$;
$y_e = y_p + d$;
if $G_i \in Area(O_1, O_2, O_3, O_4)$ **then continue**;
if $y_g \in [max\{l_1(x_g).y,\ l_2(x_g).y,\ y_o - \frac{w}{2}\},\ ye]$ **then**
SG.add(G_i);
end if
// **Type 7**:
else if $x_p < x_o - \frac{l}{2}$ & $y_p < y_o - \frac{w}{2}$ **then**
$l_1(AP, O_3)$, $l_2(AP, O_2)$, $l_3(O_2, O_3)$;
$d = \delta \cdot length(AP, O_1)$;
$K = (O_1.y - y_p)/(O_1.x - x_p)$;
$x_e = \frac{d}{\sqrt{K^2+1}} + x_p$, $y_e = \frac{K \cdot d}{\sqrt{K^2+1}} + y_p$;
if $G_i \in Area(O_1, O_2, O_3, O_4)$ **then continue**;
if $x_g \leq x_e$ & $y_g \in [max\{l_2(x_g).y,\ l_3(x_g).y\},$
$min\{l_1(x_g).y,\ ye\}]$ **then**
SG.add(G_i);
end if
// **Type 8**:
else if $x_p < x_o - \frac{l}{2}$ & $y_p \in [y_o - \frac{w}{2}, y_o + \frac{w}{2}]$ **then**
$l_1(AP, O_3)$, $l_2(AP, O_4)$;
$d = \delta \cdot (x_o + \frac{l}{2} - x_p)$;
$x_e = x_p + d$;
if $G_i \in Area(O_1, O_2, O_3, O_4)$ **then continue**;
if $x_g \in [x_o - \frac{l}{2},\ x_e]$ & $y_g \in [l_2(x_g).y,\ l_1(x_g).y]$ **then**
SG.add(G_i);
end if
// **Type 9**:
else
$x_{d_1} = max\{x_p - \delta \cdot (x_p - x_o + \frac{l}{2}),\ 0\}$;
$x_{d_2} = min\{x_p + \delta \cdot (x_o + \frac{l}{2} - x_p),\ r_l\}$;
$y_{d_1} = max\{y_p - \delta \cdot (y_p - y_o + \frac{w}{2}),\ 0\}$;
$y_{d_2} = min\{y_p + \delta \cdot (y_o + \frac{w}{2} - y_p),\ r_w\}$;
if $G_i \in Area(O_1, O_2, O_3, O_4)$ **then continue**;
if $x_g \in (x_{d_1},\ x_{d_2})$ & $y_g \in (y_{d_1},\ y_{d_2})$ **then**
SG.add(G_i);
end if
end if
return SA = $size$(SG)·l_g^2, SG;
end for

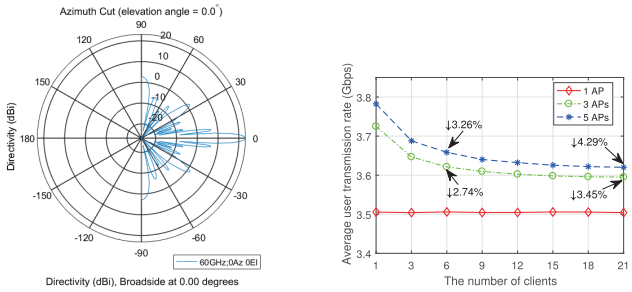

(a) Antenna directivity. (b) Network performance.

Fig. 29. (a) Antenna model and (b) performance with side-lobe effects and interference.

APPENDIX C
ANTENNA MODEL AND MULTI-LOBE EFFECTS

In this work, narrow-beam directional antennas such as those typically used on mmWave devices are assumed. Fig. 29a shows the antenna pattern produced by a 61-element uniform hexagonal array antenna. As can be seen from the figure, the main lobe has much higher antenna gain than the side lobes. Based on this directional antenna model and the sparse cluster-based channel model described in Sec. VII-A, we investigate the interference caused by both main-lobe/side-lobe emanations and reflection effects.

In this evaluation, we use the High-R Case scenario, as described in Sec. VII-A. Recall that in the High-R Case scenario, all objects in the room are highly reflective. From the environment standpoint, this can be considered a worst-case scenario for interference, since signals that reflect off obstacles will maintain close to their unreflected signal powers and will therefore produce maximum interference power at unintended destinations. In the evaluated scenario, each client associates to the best AP that provides the highest signal strength, and then is randomly allocated a specific 1-second time slot for transmission with its connected AP. In each time slot, we calculate interference power in the 3D spatial domain at each receiver caused by transmitters other than its intended transmitter by considering both main lobes and side lobes of antennas and using the aforementioned sparse cluster-based channel model with very high reflection coefficients.

Given the above scenario and with a specific mean obstacle density of $0.3/m^2$ and LoS-optimally placed APs, the average user transmission rate with a varying number of clients and APs are evaluated over 200 random obstacle and client placements,[9] and the results are reported in Fig. 29 (b). The user

[9]For multi-AP scenarios, the cases without any simultaneous transmission links are not counted in the evaluation.

transmission rate is the user throughput during its one second of active time as measured in ns-3.[10]

From Fig. 29 (b), we observe that average transmission rate degrades slightly as the number of clients and APs increases due to the interference effects, where the interference signals could be emanated from the main lobes or side lobes of antennas and arrive via LoS or reflected paths. However, due to the narrow beamwidth of the antenna, the probability of receiving interference signals from the main lobe is fairly low, and most of the unintended signals emanated and/or received by the side lobes have fairly low signal strength as compared to the intended signals. Therefore, as we see in Fig. 29 (b), the average performance degradation caused by interference effects is only around 2.1%∼4.3%. We note also that the environment simulated to obtain these results, where the room is quite densely populated with obstacles and all obstacles are highly reflective, is a very extreme one from an interference standpoint and so interference impacts in more typical environments will be even smaller.

APPENDIX D
COMPLEXITY ANALYSIS OF PROPOSED ALGORITHMS

In this work, we mainly propose four algorithms (Algorithms 1–4), and here we provide a complexity analysis of each of these algorithms.

The time complexity of Algorithm 1 is $O(N_o N_g)$, where N_o is the number of obstacles and N_g denotes the number of traversed grids, which equals to $(r_l \cdot r_w / l_g)$. Derived from Algorithm 1, the time complexity of our SES algorithm (i.e., Algorithm 2) also depends on the number of deployed APs. In the worst case, i.e. assuming the blockage-free operation is not achieved until finding all APs' positions, Algorithm 2 runs in the time complexity of $O(N_a N_o {N_g}^2)$, where N_a is the number of required APs. However, since N_a is typically a very small value, it can effectively be considered a constant and, especially when obstacle density is not very high, the time complexity is effectively $O(N_o {N_g}^2)$.

The time complexity of Algorithm 3 is $O(N_a N_o N_g N_u)$ in the worst case, where N_u is the number of known positions of users. As compared to the time complexity of Algorithm 2, Algorithm 3 runs quite fast since N_u is far smaller than N_g, which is illustrated in Fig. 29.

The time complexity of Algorithm 4 is $O({N_R N_{am} N_o {N_{gm}}^2} + N_{nR} N_o (N_{aj} N_{gj}^2 + N_{an} N_{gn}^2))$, where N_R is the number of mRRs, N_{am} and N_{gm} are the number of required APs and traversed grids in mRRs, N_{nR} is the number of non-mRRs, N_{aj} and N_{gj} are the number of APs and grids in JRs, and N_{an} and N_{gn} are the number of required APs and traversed grids in those non-mRRs. Since N_R and N_{nR} are always small values in Algorithm 4, the algorithm runs only a little bit slower than Algorithm 2 in a typical L-shaped or U-shaped room, which is actually the combination of a few rectangular rooms.

Note that all proposed algorithms are run at network deployment time, not during network operation, which makes their running time less critical.

[10]This is not the same as link transmission rate since it does not include packet header information in its calculation.

REFERENCES

[1] X. Wang *et al.*, "Millimeter wave communication: A comprehensive survey," *IEEE Commun. Surveys Tuts.*, vol. 20, no. 3, pp. 1616–1653, 3rd Quart., 2018.

[2] T. S. Rappaport *et al.*, "Millimeter wave mobile communications for 5G cellular: It will work!," *IEEE Access*, vol. 1, pp. 335–349, 2013.

[3] *IEEE std 802.11ad-2012*. Accessed: Oct. 11, 2021. [Online]. Available: https://ieeexplore.ieee.org/stamp/stamp.jsp?arnumber=6392842

[4] *Talon AD7200 Multi-Band Wi-Fi Router*. Accessed: Oct. 11, 2021. [Online]. Available: https://www.pcmag.com/review/347405/tp-link-talon-ad7200-multi-band-wi-fi-router

[5] Y. Liu and D. M. Blough, "Analysis of blockage effects on roadside relay-assisted mmWave backhaul networks," in *Proc. IEEE Int. Conf. Commun. (ICC)*, May 2019, pp. 1–7.

[6] S. Singh, F. Ziliotto, U. Madhow, E. Belding, and M. Rodwell, "Blockage and directivity in 60 GHz wireless personal area networks: From cross-layer model to multihop MAC design," *IEEE J. Sel. Areas Commun.*, vol. 27, no. 8, pp. 1400–1413, Oct. 2009.

[7] H. Zhao *et al.*, "28 GHz millimeter wave cellular communication measurements for reflection and penetration loss in and around buildings in New York city," in *Proc. IEEE Int. Conf. Commun.*, Jun. 2013, pp. 5163–5167.

[8] S. Sur, I. Pefkianakis, X. Zhang, and K.-H. Kim, "WiFi-assisted 60 GHz wireless networks," in *Proc. 23rd Annu. Int. Conf. Mobile Comput. Netw.*, Oct. 2017, pp. 28–41.

[9] P. F. M. Smulders, "Statistical characterization of 60-GHz indoor radio channels," *IEEE Trans. Antennas Propag.*, vol. 57, no. 10, pp. 2820–2829, Oct. 2009.

[10] W. Li, L. Tian, J. Zhang, and Y. Cheng, "Analysis of base station deployment impact on LOS probability model for 5G indoor scenario," in *Proc. IEEE/CIC Int. Conf. Commun. China*, Oct. 2017, pp. 1–5.

[11] X. Qin, X. Yuan, Z. Zhang, F. Tian, Y. T. Hou, and W. Lou, "On AP assignment and transmission scheduling for multi-AP 60 GHz WLAN," in *Proc. IEEE 14th Int. Conf. Mobile Ad Hoc Sensor Syst. (MASS)*, Oct. 2017, pp. 189–197.

[12] S. Sur, I. Pefkianakis, X. Zhang, and K.-H. Kim, "Towards scalable and ubiquitous millimeter-wave wireless networks," in *Proc. 24th Annu. Int. Conf. Mobile Comput. Netw.*, Oct. 2018, pp. 257–271.

[13] R. Singh and D. Sicker, "SHINE (strategies for high-frequency INdoor environments) with efficient THz-AP placement," in *Proc. IEEE 91st Veh. Technol. Conf. (VTC-Spring)*, May 2020, pp. 1–7.

[14] S. Chatterjee, M. J. Abdel-Rahman, and A. B. MacKenzie, "Robust access point deployment and adaptive user assignment for indoor millimeter wave networks," in *Proc. IEEE Int. Conf. Commun.*, Jun. 2020, pp. 1–6.

[15] S. Chatterjee, M. J. Abdel-Rahman, A. B. MacKenzie, and A. B. MacKenzie, "A joint optimization framework for network deployment and adaptive user assignment in indoor millimeter wave networks," *IEEE Trans. Wireless Commun.*, early access, Jul. 12, 2021, doi: 10.1109/TWC.2021.3085563.

[16] Y. Lee, K. Kim, and Y. Choi, "Optimization of AP placement and channel assignment in wireless LANs," in *Proc. 27th Annu. IEEE Conf. Local Comput. Netw. (LCN)*, Nov. 2002, pp. 831–836.

[17] M. N. Soorki, M. J. Abdel-Rahman, A. MacKenzie, and W. Saad, "Joint access point deployment and assignment in mmWave networks with stochastic user orientation," in *Proc. IEEE Model. Optim. Mobile, Ad Hoc, Wireless Netw.*, May 2017, pp. 1–6.

[18] M. N. Soorki, W. Saad, and M. Bennis, "Optimized deployment of millimeter wave networks for in-venue regions with stochastic Users' orientation," *IEEE Trans. Wireless Commun.*, vol. 18, no. 11, pp. 5037–5049, Nov. 2019.

[19] T. Wei, A. Zhou, and X. Zhang, "Facilitating robust 60 GHz network deployment by sensing ambient reflectors," in *Proc. USENIX Symp. Netw. Syst. Design Implement.*, 2017, pp. 213–226.

[20] M. Park and H. K. Pan, "A spatial diversity technique for IEEE 802.11ad WLAN in 60 GHz band," *IEEE Commun. Lett.*, vol. 16, no. 8, pp. 1260–1262, Aug. 2012.

[21] X. Zhou *et al.*, "Mirror mirror on the ceiling: Flexible wireless links for data centers," *ACM SIGCOMM Comput. Commun. Rev.*, vol. 42, no. 4, pp. 443–454, Sep. 2012.

[22] A. Deng, Y. Liu, and D. M. Blough, "Maximizing coverage for mmWave WLANs with dedicated reflectors," in *Proc. IEEE Int. Conf. Commun. (ICC)*, Jun. 2021, pp. 1–6.

[23] M. K. Samimi and T. S. Rappaport, "Characterization of the 28 GHz millimeter-wave dense urban channel for future 5G mobile cellular," NYU Wireless TR, New York, NY, USA, Tech. Rep. 1, 2014.
[24] Q. Wu, S. Zhang, B. Zheng, C. You, and R. Zhang, "Intelligent reflecting surface-aided wireless communications: A tutorial," *IEEE Trans. Commun.*, vol. 69, no. 5, pp. 3313–3351, May 2021.
[25] S. Zeng, H. Zhang, B. Di, Z. Han, and L. Song, "Reconfigurable intelligent surface (RIS) assisted wireless coverage extension: RIS orientation and location optimization," *IEEE Commun. Lett.*, vol. 25, no. 1, pp. 269–273, Jan. 2021.
[26] Z. Yang, P. H. Pathak, J. Pan, M. Sha, and P. Mohapatra, "Sense and deploy: Blockage-aware deployment of reliable 60 GHz mmWave WLANs," in *Proc. IEEE Mobile Ad Hoc Sensor Syst.*, Oct. 2018, pp. 397–405.
[27] Y. Niu, Y. Li, D. Jin, L. Su, and D. Wu, "Blockage robust and efficient scheduling for directional mmWave WPANs," *IEEE Trans. Veh. Technol.*, vol. 64, no. 2, pp. 728–742, Feb. 2015.
[28] K. Song, R. Cai, and D. Liu, "A fast relay selection algorithm over 60 GHz mm-wave systems," in *Proc. 15th IEEE Int. Conf. Commun. Technol.*, Nov. 2013, pp. 676–680.
[29] O. Abari, "Enabling high-quality untethered virtual reality," in *Proc. 1st ACM Workshop Millim.-Wave Netw. Sens. Syst.*, Oct. 2017, pp. 531–544.
[30] N. Chatzipanagiotis and M. M. Zavlanos, "Distributed scheduling of network connectivity using mobile access point robots," *IEEE Trans. Robot.*, vol. 32, no. 6, pp. 1333–1346, Dec. 2016.
[31] Y. Jian, Y. Liu, S. K. Venkateswaran, D. M. Blough, and R. Sivakumar, "A quantitative exploration of access point mobility for mmWave WiFi networks," in *Proc. IEEE Int. Conf. Commun. (ICC)*, Jun. 2020, pp. 1–7.
[32] Y. Jian, M. Agarwal, S. K. Venkateswaran, Y. Liu, D. M. Blough, and R. Sivakumar, "WiMove: Toward infrastructure mobility in mmWave WiFi," in *Proc. 18th ACM Symp. Mobility Manage. Wireless Access*, Nov. 2020.
[33] Y. Jian, M. Agarwal, Y. Liu, D. M. Blough, and R. Sivakumar, "Poster: Hawkeye–predictive positioning of a ceiling-mounted mobile AP in mmWave WLANs for maximizing line-of-sight," in *Proc. 25th Annu. Int. Conf. Mobile Comput. Netw.*, Oct. 2019, pp. 1–3.
[34] F. Zhou, M. Y. Naderi, K. Sankhe, and K. Chowdhury, "Making the right connections: Multi-AP association and flow control in 60 GHz band," in *Proc. IEEE Conf. Comput. Commun. (INFOCOM)*, Apr. 2018, pp. 1214–1222.
[35] G. Athanasiou, P. C. Weeraddana, C. Fischione, and L. Tassiulas, "Optimizing client association for load balancing and fairness in millimeter-wave wireless networks," *IEEE/ACM Trans. Netw.*, vol. 23, no. 3, pp. 836–850, Jun. 2015.
[36] R. Cowan, "Objects arranged randomly in space: An accessible theory," *Adv. Appl. Probab.*, vol. 21, no. 3, pp. 543–569, Sep. 1989.
[37] T. Bai, R. Vaze, and R. W. Heath, Jr., "Analysis of blockage effects on urban cellular networks," *IEEE Trans. Wireless Commun.*, vol. 13, no. 9, pp. 5070–5083, Sep. 2014.
[38] A. Heppes and H. Melissen, "Covering a rectangle with equal circles," *Periodica Mathematica Hungarica*, vol. 34, nos. 1–2, pp. 65–81, 1997.
[39] J. B. M. Melissen and P. C. Schuur, "Covering a rectangle with six and seven circles," *Discrete Appl. Math.*, vol. 99, nos. 1–3, pp. 149–156, Feb. 2000.
[40] H. Assasa and J. Widmer, "Implementation and evaluation of a WLAN IEEE 802.11ad model in ns-3," in *Proc. Workshop*, 2016, pp. 57–64.
[41] H. Assasa, J. Widmer, T. Ropitault, and N. Golmie, "Enhancing the ns-3 IEEE 802.11 ad model fidelity: Beam codebooks, multi-antenna beamforming training, and quasi-deterministic mmwave channel," in *Proc. Workshop*, 2019, pp. 33–40.
[42] D. Halperin, S. Kandula, J. Padhye, P. Bahl, and D. Wetherall, "Augmenting data center networks with multi-gigabit wireless links," *ACM SIGCOMM Comput. Commun. Rev.*, vol. 41, no. 4, pp. 38–49, Oct. 2011.
[43] Y. Liu, Y. Jian, R. Sivakumar, and D. M. Blough, "Optimal access point placement for multi-AP mmWave WLANs," in *Proc. 22nd Int. ACM Conf. Modeling, Anal. Simul. Wireless Mobile Syst. (MSWIM)*, 2019, pp. 35–44.
[44] E. Perahia, "TGad evaluation methodology," in *Proc. IEEE P802.11 Wireless LANs*, Jan. 2009, pp. 1–16.
[45] X. Wu *et al.*, "60-GHz millimeter-wave channel measurements and modeling for indoor office environments," *IEEE Trans. Antennas Propag.*, vol. 65, no. 4, pp. 1912–1924, Apr. 2017.
[46] Y. Shoji, H. Sawada, C.-S. Choi, and H. Ogawa, "A modified SV-model suitable for line-of-sight desktop usage of millimeter-wave WPAN systems," *IEEE Trans. Antennas Propag.*, vol. 57, no. 10, pp. 2940–2948, Oct. 2009.
[47] A. Maltsev, R. Maslennikov, A. Sevastyanov, A. Khoryaev, and A. Lomayev, "Experimental investigations of 60 GHz WLAN systems in office environment," *IEEE J. Sel. Areas Commun.*, vol. 27, no. 8, pp. 1488–1499, Oct. 2009.

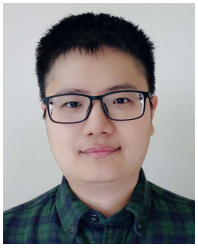

Yuchen Liu (Graduate Student Member, IEEE) received the B.S. degree in electrical and computer engineering from Shanghai University in 2014 and the M.S. degree in electrical and computer engineering from Shanghai Jiao Tong University, China, in 2017. He is currently pursuing the Ph.D. degree in electrical and computer engineering with the Georgia Institute of Technology, USA. His research interests are in the area of wireless networking, millimeter-wave communications, and network intelligence.

Yubing Jian received the B.S. degree (Hons.) in electronics and communications engineering from the University of Bristol, Bristol, U.K., in 2013, and the M.S. and Ph.D. degrees from the Department of Electrical and Computer Engineering, Georgia Institute of Technology, Atlanta, USA, in 2015 and 2020, respectively. His research interests are broadly within the area of wireless communications, computer networks, and molecular communications.

Raghupathy Sivakumar (Fellow, IEEE) received the B.E. degree in computer science from the College of Engineering, Anna University, Chennai, in 1996, and the M.S. and Ph.D. degrees in computer science from the University of Illinois at Urbana-Champaign in 1998 and 2000, respectively. He is the Wayne J. Holman Chair Professor with the School of Electrical and Computer Engineering, Georgia Tech. He leads the Georgia Tech Networking and Mobile Computing Research Group, where he and his students do research in the areas of wireless networking, mobile computing, and computer networks.

Douglas M. Blough (Senior Member, IEEE) received the B.S. degree in electrical engineering, and the M.S. and Ph.D. degrees in computer science from Johns Hopkins University in 1984, 1986, and 1988, respectively. He is currently a Professor of electrical and computer engineering with the Georgia Institute of Technology. His research considers a variety of problems in computer networks with a primary interest in advanced wireless networking techniques.